Research Square

Preprints are preliminary reports that have not undergone peer review.
They should not be considered conclusive, used to inform clinical practice,
or referenced by the media as validated information.

Application of Multi-Layer Particle Swarm Optimization Algorithm for ORPD in Renewable-Integrated Power Systems Incorporating FACTS Devices

Avinash Kumar
SRM Institute of Science and Technology
Saptarshi Gupta
SRM Institute of Science and Technology
Rupali Singh
SRM Institute of Science and Technology
Dharmbir Prasad
SRM Institute of Science and Technology
Pankaj Kumar
k.pankaj@manipal.edu

Manipal Institute of Technology, Manipal Academy of Higher Education

Article

Keywords: Reactive power, optimal dispatch, renewable energy, wind power, solar PV, multi-layer PSO, FACTS devices, statistical analysis, contingency

Posted Date: June 30th, 2026

DOI: https://doi.org/10.21203/rs.3.rs-10030899/v1

License: This work is licensed under a Creative Commons Attribution 4.0 International License.
Read Full License

Additional Declarations: No competing interests reported.

Application of Multi-Layer Particle Swarm Optimization Algorithm for ORPD in Renewable-Integrated Power Systems Incorporating FACTS Devices

Avinash Kumar[1], Saptarshi Gupta[2], Rupali Singh[3], Dharmbir Prasad[4], Pankaj Kumar[5*]

[1]Department of Electrical and Electronics Engineering, SRM Institute of Science and Technology, Modinagar, PIN-201204, Uttar Pradesh, India, Email: ak6477@srmist.edu.in
[2]Department of Electronics and Communication Engineering, Faculty of Engineering and Technology, SRM Institute of Science and Technology, Delhi-NCR Campus, Modinagar, Ghaziabad 201204, Uttar Pradesh, India, Email: saptarsg@srmist.edu.in
[3]Department of Electronics and Communication Engineering, Faculty of Engineering and Technology, SRM Institute of Science and Technology, Delhi-NCR Campus, Modinagar, Ghaziabad 201204, Uttar Pradesh, India, Email: rupalis@srmist.edu.in
[4]Department of Electrical and Electronics Engineering, Faculty of Engineering and Technology, SRM Institute of Science and Technology, Delhi-NCR Campus, Modinagar, Ghaziabad 201204, Uttar Pradesh, India, Email: dharmbirprasad@yahoo.com
*[*5]Manipal Institute of Technology, Manipal Academy of Higher Education, Manipal, India, Email: k.pankaj@manipal.edu*

Abstract

The increasing penetration of wind and solar generation into modern power grids has raised a bigger challenge in voltage control and reactive power management owing to the intermittent characteristic and limited reactive power capacity of the inverter-based resources. To address this kind of optimal reactive power dispatch (ORPD) problem, this paper adopts a recently developed multi-layer particle swarm optimization (MLPSO) algorithm for solving the same in a renewable-integrated system along with flexible AC transmission systems (FACTS) devices. The classical ORPD model is generalized by the choice of the reactance of thyristor-controlled series capacitors (TCSCs) and the angle of phase shifting of thyristor-controlled phase shifters (TCPSs) as additional decision variables with operating limits included explicitly in the constraints. Testing is carried out on a modified IEEE 30-bus network, in which generators at buses-8 (*viz.,* source: solar PV), -11, and -13 (*viz.,* source: wind farms) are simulated as renewable energy (RE) plants. The numerical studies are carried out in four scenarios: without FACTS devices, two TCSCs, two TCSCs and a single TCPS, three TCSCs and three TCPSs. Here, minimization of two different objectives is performed: real power loss and total bus voltage deviation. Compared with some recent past results by real-coded genetic algorithm (RCGA), differential evolution (DE), and biogeography-based optimization (BBO), the MLPSO obtains smaller active power loss as well as voltage

deviation in all studied scenarios. Furthermore, statistical sensitivity and contingency analysis were performed. The findings demonstrate the potential of a novel algorithm to provide optimal solutions for reactive power planning in future renewable-based grids with FACTS devices.

Keywords: Reactive power, optimal dispatch, renewable energy, wind power, solar PV, multi-layer PSO, FACTS devices, statistical analysis, contingency.

Nomenclature

a_i, b_i, c_i	generator cost coefficients
c_1, c_2	cognitive and social coefficients
d_i, e_i	valve-point loading effect coefficients
B_{ij}	line charging susceptance
f	system frequency
g_{ij}^{best}	global best position
g_{suc}, l_{suc}	success counters for global and local variants
G_{ij}	conductance of line $i-j$
k	neighbourhood radius
L-index	voltage stability index
m	number of layers in MLPSO
N_b	number of buses
N_c	number of shunt compensators
N_g	number of generator buses
N_l	number of transmission lines
N_{size}	total population size
N_t	number of transformers
N_{TCPS}	number of TCPS devices
N_{TCSC}	number of TCSC devices
p_g, p_l	global and local selection probabilities
P_{Di}, Q_{Di}	active and reactive power demand at bus i
P_{Gi}, Q_{Gi}	active and reactive power generation at bus i
$P_{Gi}^{min}, P_{Gi}^{max}$	minimum and maximum active power limits
p_{ij}^{best}	personal best position

P_{ij}, Q_{ij}	active and reactive power flow from bus i to j
$Q_{C_i}^{min}, Q_{C_i}^{max}$	minimum and maximum shunt compensator limits
P_{Loss}	active power loss
P_{ns}	neighbourhood search probability
Q_{C_i}	shunt compensator reactive output
$Q_{Gi}^{min}, Q_{Gi}^{max}$	minimum and maximum reactive power limits
$r_1, r_2, r_3, r_4, r_5, r_6$	random weights in LNS and GNS
R_{ij}, X_{ij}	resistance and reactance of line $i-j$
S_{ij}	apparent power flow in line $i-j$
S_P	swarm-particle distribution per layer
S_{ij}^{max}	maximum apparent power flow limit
TVD	total voltage deviation
T_i	transformer tap setting
T_i^{min}, T_i^{max}	minimum and maximum transformer tap limits
V_{G_i}	generator voltage at bus i
V_i^{min}, V_i^{max}	minimum and maximum voltage limits at bus i
V_i	voltage magnitude at bus i
w	inertia weight in PSO
$X_{C_{ij}}$	TCSC reactance between buses i and j
x_{ij}, v_{ij}	position and velocity of particle i in dimension j
$X_{C_{ij}}^{min}, X_{C_{ij}}^{max}$	minimum and maximum TCSC reactance limits
Y_{ij}	admittance of line $i-j$
θ_i	voltage angle at bus i
θ_{ij}	admittance angle
ϕ_{ij}	TCPS phase shift angle between buses i and j
$\phi_{ij}^{min}, \phi_{ij}^{max}$	minimum and maximum TCPS phase shift limits
α, ϕ, γ	MLPSO algorithm parameters
$\Delta\delta$	rotor angle deviation
ABC	artificial bee colony
AEFA-FDB	artificial electric field algorithm–fitness distance balance
ALO	ant lion optimizer

BBO	biogeography-based optimization
CAC-DE	continuous ant colony–differential evolution
CCT	critical clearing time
CPU	central processing unit
DE	differential evolution
DFIG	doubly-fed induction generator
EPRI	Electric Power Research Institute
FACTS	flexible ac transmission systems
GA	genetic algorithm
GJSO	gradient jellyfish search optimizer
GNS	global neighbourhood search
GSA	gravitational search algorithm
IMPA	improved marine predators' algorithm
LNS	local neighbourhood search
MLPSO	multi-layer particle swarm optimization
NR	Newton-Raphson
ORPD	optimal reactive power dispatch
PV	photovoltaic
RCGA	real-coded genetic algorithm
RE	renewable energy
RES	renewable energy sources
RoCoF	rate of change of frequency
TCSC	thyristor-controlled series capacitor
TCPS	thyristor-controlled phase shifter
TVD	total voltage deviation
PSO	particle swarm optimization
PSOIWA	particle swarm optimization with inertia weight approach
SHADE	success history-based adaptive differential evolution
WOA	whale optimization algorithm

1. Introduction

1.1 Problem definition

It is important to manage the reactive power resources for stability and security of power systems, particularly when renewable energies like wind and solar-PV systems are being penetrated into the grid, which brings in uncertainties and a limited provision of VAr support from inverter-based interfaces [1]. ORPD is one of the tools, which attempts to determine the control settings for reactive power generation to optimise a particular objective function (e.g., minimisation in real power flow losses and total voltage deviation) over some parameters space and subject to several equality/inequality constraints such as: power flow equations, upper/lower limit on voltage magnitude and capacity constraints, existent on several reactive resources i.e., generating units, shunt capacitor banks and transformer taps [2],etc. In the last few years, rapid developments in power electronics and microelectronics have given rise to a new possibility of more flexible control of power systems, particularly for integration with high penetration ratios of renewable energy sources. The term FACTS,also countedas a sub-area of power electronics-based controllers, refers to the control of power using advanced solid-state and microchip-based electronic devices for high-voltage electrical energy transit. The FACTS device was developed by EPRI [3] to create a series of these control loops. These new devices have resulted in the existing transmission and distribution of electricity becoming more reliable, more controllable, and a lot more efficient [4], which can be utilised to provide improved voltage regulation for renewables-based networks. But the FACTS devices are mostly intended to allow maximum utilization of the existing transmission facilities subject to the limits imposed by concerns of reliability, loop flow and sub synchronous resonance (e.g., solution to solve stability problem as well) and very limited efforts have been made in academia for analysing the effect of FACTS device on improving static performance like cost and loss minimization in renewable integrated scenario [5, 6].

1.2 Background perspective

In the past, several conventional as well as evolutionary optimization algorithms such as linear programming [2], nonlinear programming [7], quadratic programming [8, 9] Newton approach [10], interior point methods [11], genetic algorithm (GA) [12], improved GA [13], adaptive GA [14], evolutionary programming [15], differential evolution (DE) [16], real-coded GA (RCGA) [17], self-adaptive RGA [18], particle swarm optimization (PSO) [19], seeker optimization algorithm [20], biogeography-based optimization (BBO) [21], gravitational search algorithm (GSA) [22], opposition based GSA [23], hybrid Nelder-Mead simplex based firefly algorithm [24], etc have been, successfully, applied to solve the ORPD problem of power systems.Some optimization techniques such as GA [25], DE [25], PSO

[25], multi-objective evolutionary algorithm [26], RCGA [27], PSO with inertia weight approach (PSOIWA) and BBO etc [27]have already been presented in the literature for solving ORPD problem of power systems under FACTS devices while extensions have also been carried out to incorporate renewable energy integration in recent works by Das et al.[28]. PSO is a recently developed optimization technique for modelling the swarm behaviour of birds searching for food, which has attracted more attention due to its freshness and search ability. PSO has been applied to a wide range of fields in power systems, as reported in [29]. However, this method has its own limitations and could easily get stuck in a local optimum when it is used to solve complex multimodal problems. It can also beaffected by the "explosion" phenomenon [30]. Therefore, continuous attention is being given by the research community to its further enhancement, especially for addressing uncertainties in renewable-dominated grids [31].

The ORPD problem, a non-linear, non-convex, mixed-integer optimization challenge in power systems, seeks to optimally adjust control variables like generator voltages, transformer taps, and shunt compensators to minimize active power losses, voltage deviations, and enhance voltage stability under operational constraints; over the period 2015-2025, metaheuristic algorithms have progressively dominated its solution, starting with early nature-inspired approaches such as chaotic krill herd algorithm (CKHA) [32] achieving superior loss minimization and stability enhancement, Gaussian bare-bones water cycle algorithm (NGBWCA) [33] effectively mitigating premature convergence on IEEE 30-/57-/118-bus systems, Whale Optimization Algorithm (WOA) [34]proving robust on the Algerian 114-bus system, Ant Lion Optimizer (ALO) [35] excelling in large-scale IEEE 300-bus cases, hybrid PSO-Multi Verse Optimizer (HPSO-MVO) [36] delivering multi-objective improvements, and Artificial Bee Colony (ABC) [37] enhancing loss/voltage/stability metrics, before advancing to stochastic formulations that incorporate renewable uncertainties via Success History-based Adaptive Differential Evolution (SHADE) with scenario-based wind/solar modelling [38], Two-Point Estimate Method for load uncertainty in multi-objective setups [39, 40], Improved Marine Predators Algorithm (IMPA) [41] avoiding local optima entrapment, Hybrid Continuous Ant Colony-Differential Evolution (CAC-DE) [42] yielding 27-39% greater loss reductions than MODE/SPEA2, and semidefinite programming ensuring global optimality [43]; more recent innovations (2024-2025) include Gradient Jellyfish Search Optimizer (GJSO) [44] outperforming in accuracy and stability, Modified Artificial Hummingbird Algorithm [45] excelling in solar/wind/hydro integration, Adaptive

Beluga Whale Optimization [46] significantly reducing expected losses and deviations with UPFC inclusion, AEFA-FDB [47] attaining minimal losses (e.g., 4.4138 MW on IEEE 30-bus) with 18-43% average improvements, JAYA variants [48-50] producing optimal losses (e.g., 1.8641 MW) under wind/load uncertainties and up to 59% reductions in hybrid HVAC-HVDC configurations, reserve-constrained Grey Wolf Optimizer [51] achieving 25.8% loss reduction and 32.8% stability gains, and multi-objective models integrating wind/PV/FACTS/emissions/costs [28] realizing 4.97-31.38% improvements collectively demonstrating a clear evolution toward hybrid, chaos-enhanced, multi-objective, and uncertainty-aware metaheuristics that deliver substantial loss reductions, superior voltage profiles, robust renewable energy integration (e.g., wind, solar, PV, hydro, tidal), and enhanced system security across standard and real-world test systems, thereby advancing sustainable and reliable power system operation.

1.3 Motivation of the present work

Notwithstanding the many successful developments on PSO and its variants, primitive PSO and many of its initial modifications both have two basic deficiencies: premature attainment of sub-optimal solutions and slow convergence speed, especially for highly complex, multi-modal, non-linear, constrained real-world optimization problems [52, 53]. Furthermore, these limitations become more pronounced in benchmark power system problems used by recent studies, such as ORPD for renewable integrated systems with high concentrations of intermittent wind and solar generation, along with complications arising from the inclusion of FACTS devices (viz., TCSC, TCPS). Such problems feature:

- large-scale, high-dimensional decision spaces,
- non-convex cost functions (minimizing P_{Loss}, minimizing TVD),
- multiple conflicting objectives,
- stochastic uncertainties from renewable sources,
- equality and inequality constraints (power flow equation, device constraints).

To overcome such challenges, two primary improvements have been incorporated into the traditional PSO-based framework, which builds upon a recent MLPSO method proposed by Tran and Wu [54]. A multi-layer search heuristic that adaptively combines global exploration and local exploitation by the dynamic switching of the search layers and neighbourhood topologies.

The rapid injection of wind and solar power into the system has resulted in an increased demand for improved reactive power control based on their intermittent nature and low levels of inverter support. In the literature, several different strategies based on mutual coordination of the renewable energy sources (RES) and FACTS controllers, such as to enhance ORPD were proposed. A comprehensive review by Adegoke et al. [55] indicated that the use of RES combined with TCSC, SVC, UPFC, and STATCOM significantly improves the voltage stability as well as reduces the loss, too, by mentioning that the best solution is obtained by hybrid or advanced meta-heuristic techniques. Naderi et al. [56] applied a hybrid Wavelet-Mutated-Shuffled Frog Leaping and PSO to solve multi-objective optimal power flow in the presence of TCSC and UPFC, which is better than classical approaches from the point of view of convergence rate and solution quality. Banerjee et al. [57] convincingly hedged uncertainty of probabilistic wind, solar, and EV in a large-scale network (*e.g.,* IEEE 118-bus) upon précised positioning of SSSC and UPFC with an improved meta-heuristic technique, proving the significance of multi-series/shunt FACTS in renewable-enabled networks. Rani and Malakar [31] presented reserve-constrained ORPD for wind integrated grid with coronavirus flock immunity optimizer, based on those reactive reserves need to be maintained adequately due to the uncertainty of system gap by FACTS compensation vacuum. Meanwhile, Cheng et al. [58], Meng et al. [59], and Roy and Das [6] studied game-theoretic, flexibility index-based, and droop-controlled islanded strategies motivated by the fact that optimization techniques robust to a variety of uncertainty (and also sophisticated compensation equipment) are needed for modern renewable-rich grids. However, there are limited works that integrate multi-bus-based realistic inverter-constrained renewable models, multiple TCSC and TCPS devices, and a latest-generation multi-layer PSO framework on the benchmark IEEE 30 bus modified system with intact original reactive limits to have a fair comparison. This is actually where the current study is trying to bridge the gap.

1.4 Contribution of the present study

In this work, integration of two FACTS devices (*i.e.,* TCSC and TCPS) into the ORPD problem at various locations within the power network under consideration is considered in order to account for renewable energy sources. In this study, the minimization of both P_{Loss} and $TVD$is considered separately using power balance, active and reactive power generation limits, voltage profiles, transmission line loading constraints, and FACTS parameters

constraints. The application performance of the proposed MLPSO is demonstrated through results obtained from the modified IEEE-30 bus test power system with renewable integration. The obtained results are also compared with other computational intelligence-based methods emerged in recent literature [1].

1.5 Layout of the paper

The rest of this paper is structured as follows. FACTS devices modelling is described in Section-2. The mathematical problem of the ORPD with FACTS is addressed in Section-3. The MLPSO method is presented in Section-4. Simulation results are depicted, and their discussion can be found in Section-5. Further, sensitivity and robustness analysis are illustrated in Section-6. Summary and concluding remarks of the current work are made in Section-7.

2.Modelling of FACTS devices

For TCSC and TCPS, the proposed models are based on steady-state models that follow the approach of power-injection and the branch model, which is commonly reported in literature. These models are also applicable regardless of generation topology (e.g., synchronous or renewable based on the inverter side connected to the system), because FACTS controllers directly affect the transmission line parameters and bus voltages.

2.1 Modelling of the TCSC device

In renewable integrated power systems, TCSC is of paramount importance in real-time line reactance compensation, thus minimizing the real power loss, enhancing voltage profiles, and eliminating congestion due to variable wind and solar generation. Contrary to inverter-based reactive support from renewables, the fast response capacity and wide operating range of TCSC render it very effective for steady state as well as transient voltage control. The real power transmission on the compensated line can be sustained at a predetermined level over wide operating conditions [60-62]. The static model of the network with TCSC installed between the *i*-th and *j*-th bus is depicted in Fig. 1 [60-62]. The power flow equations of the branch having TCSC are given by (1)-(2) [27],

Fig. 1

$$P_{ij} = V_i^2 G_{ij} - V_i V_j G_{ij} \cos(\delta_i - \delta_j) - V_i V_j B_{ij} \sin(\delta_i - \delta_j) \quad (1)$$

$$Q_{ij} = -V_i^2 B_{ij} - V_i V_j G_{ij} \sin(\delta_i - \delta_j) + V_i V_j B_{ij} \cos(\delta_i - \delta_j) \quad (2)$$

Similarly, the real and reactive power flows from the *j*-th to the *i*-th bus may be expressed by (3)-(4), respectively,

$$P_{ji} = V_j{}^2 G_{ij} - V_i V_j G_{ij} \cos(\delta_i - \delta_j) + V_i V_j B_{ij} \sin(\delta_i - \delta_j) \quad (3)$$

$$Q_{ji} = -V_j{}^2 B_{ij} + V_i V_j G_{ij} \sin(\delta_i - \delta_j) + V_{ij} V_j B_{ij} \cos(\delta_i - \delta_j) \quad (4)$$

where,

$$\text{Conductance of transmission line } (G_{ij}) = \frac{R_{ij}}{R_{ij}{}^2 + (X_{ij} - X_{C_{ij}})^2} \quad (5)$$

$$\text{Susceptance of transmission line } (B_{ij}) = \frac{X_{ij} - X_{C_{ij}}}{R_{ij}{}^2 + (X_{ij} - X_{C_{ij}})^2} \quad (6)$$

P_{ij}, Q_{ij} : active and reactive power flows, respectively, between the *i*-th and the *j*-th bus

V_i, V_j : voltage magnitudes at the *i*-th and the *j*-th bus, respectively

δ_i, δ_j : angles at the *i*-th and the *j*-th bus, respectively

R_{ij}, X_{ij} : resistance and reactance, respectively, of the transmission line connected between the *i*-th and the *j*-th bus

$X_{C_{ij}}$: reactance of TCSC placed in the transmission line connected between the *i*-th and *j*-th bus

TCSC reactance is limited within [- $0.8X_{C_{ij}}$, 0.2 $X_{C_{ij}}$] (*i.e.,* 20% inductive to 80% capacitive compensation), which is common and popular in both conventional grid and renewable-penetrated grid.

2.2 Modelling of the TCPS device **Fig. 2**

In renewable-integrated systems, TCPS is particularly beneficial as it can control both active power flow (to alleviate variable wind/solar-based congestions) and fast reactive compensation via voltage angle adjustment for improved voltage stability without depending on the insufficient inverter capacity of the renewable generator. The static model of a TCPS, connected between the *i*-th and *j*-th bus, having a complex tapping ratio of $1:1\angle\phi$ and series admittance of $Y_{ij} = \left(G_{ij} - sqrt(-1)\, B_{ij}\right)$, is shown in Fig. 2 [60-62]. Similar to TCSC, the real

Fig. 2

and reactive power flows from the *i*-th to *j*-th bus may be expressed by (7)-(8) [27], respectively,

$$P_{ij} = \frac{V_i^2 G_{ij}}{\cos^2 \phi} - \frac{V_i V_j}{\cos \phi}\left[G_{ij} \cos(\delta_i - \delta_j + \phi) + B_{ij} \sin(\delta_i - \delta_j + \phi)\right] \quad (7)$$

$$Q_{ij} = -\frac{V_i^2 B_{ij}}{\cos^2 \phi} - \frac{V_i V_j}{\cos \phi}\left[G_{ij} \sin(\delta_i - \delta_j + \phi) - B_{ij} \cos(\delta_i - \delta_j + \phi)\right] \quad (8)$$

Similarly, the real and reactive power flows from the *j*-th to the *i*-th bus may be expressed by (9)-(10) [27], respectively,

$$P_{ji} = V_j^2 G_{ij} - \frac{V_i V_j}{\cos \phi}\left[G_{ij} \cos(\delta_i - \delta_i + \phi) - B_{ij} \sin(\delta_i - \delta_j + \phi)\right] \quad (9)$$

$$Q_{ji} = -V_j^2 B_{ij} + \frac{V_i V_j}{\cos \phi}\left[G_{ij} \sin(\delta_i - \delta_j + \phi) + B_{ij} \cos(\delta_i - \delta_j + \phi)\right] \quad (10)$$

The injected power model of TCPS is shown in Fig. 3 [60-62]. The injected real and reactive powers of TCPS at the *i*-th and *j*-th bus may be represented by (11)-(14),

Fig. 3

$$P_{ik} = -G_{ij} V_i^2 \tan^2 \phi - V_i V_j \tan \phi\left[G_{ij} \sin(\delta_i - \delta_j) - B_{ij} \cos(\delta_i - \delta_j)\right] \quad (11)$$

$$Q_{ik} = B_{ij} V_i^2 \tan^2 \phi + V_i V_j \tan \phi\left[G_{ij} \cos(\delta_i - \delta_j) + B_{ij} \sin(\delta_i - \delta_j)\right] \quad (12)$$

$$P_{jk} = -V_i V_j \tan \phi\left[G_{ij} \sin(\delta_i - \delta_j) + B_{ij} \cos(\delta_i - \delta_j)\right] \quad (13)$$

$$Q_{jk} = -V_i V_j \tan \phi\left[G_{ij} \cos(\delta_i - \delta_j) - B_{ij} \sin(\delta_i - \delta_j)\right] \quad (14)$$

All the variables keep their usual sense as in Section 2.1. Practically $|\varphi| \leq 15°$ is the operating range of the phase angle, which makes it applicable for both conventional and renewable energy-based systems.

3. Problem formulation of ORPD with FACTS for RE Integration

The ORPD problem is modelled as a large-scale, non-linear, non-convex optimization problem in order to minimize the active power transmission losses and/or total voltage deviation while meeting all operational constraints of modern microgrid, such as both conventional synchronous generators and inverter-based renewable energy sources (e.g., wind generator and solar PV). The single-line diagram of the modified IEEE 30-bus RE integrated test system is depicted in Fig. 4. To simulate grids compatible with renewable integration, the modified IEEE 30-bus test system is configured as follows: bus-8: solar PV

plant; buses-11 and -13: doubly-fed induction generator (DFIG) wind farms. The real power production, in addition to the reactive power constraints of these renewable turbines are equivalent to synchronous machines, so that the comparison between test results and values available from literature holds valid. This adjustment maintains the power flow base case in the analysis while also accurately depicting a network with high renewable penetration for which reactive support from generators is only partially constrained due to inverters.

The ORPD problem focuses on the optimization of the steady-state operational performance of a power system based on a given objective function and several equality and inequality constraints. Mathematical formulation ORPD problem [27, 48, 54] can be expressed as equations (15)-(17),

Minimize $J(\boldsymbol{x}, \boldsymbol{u})$ (15)

subject to $eq(\boldsymbol{x}, \boldsymbol{u}) = 0$ (16)

and $ieq(\boldsymbol{x}, \boldsymbol{u}) \leq 0$ (17)

The vector of dependent variables $\boldsymbol{x}$ may be represented by (18),

$$\boldsymbol{x}^T = [V_{L_1}, \cdots, V_{L_{NL}}, Q_{G_1}, \cdots, Q_{G_{NG}}, S_{l_1}, \cdots, S_{l_{NTL}}] \quad (18)$$

Similarly, the vector of control variables $\boldsymbol{u}$ may be written as in (19),

$$\boldsymbol{u}^T = [V_{G_1}, \cdots, V_{G_{NG}}, T_1, \cdots, T_{NT}, Q_{C_1}, \cdots, Q_{C_{NC}}] \quad (19)$$

where,

NG : number of generator buses
NL : number of load buses
NTL : number of transmission lines
NT : number of regulating transformers
NC : number of shunt compensators

3.1 Constraints

The ORPD problem is formulated into a set of equality and inequality constraints related to conventional power system operation and renewable-integrated networks with FACTS devices [27, 28, 49]. The ORPD with TCSC and TCPS are subjected to the constraints mentioned in the next two sub-sections.

3.1.1 Equality constraints

These constraints ensure the fulfillment of active and reactive power balancing at each bus in the renewable-integrated IEEE 30-bus modified system. The system equations are the same

as in classical power flow calculations; only the admittance matrix will automatically take into consideration TCSC reactance and TCPS phase-shift effects. These constraints represent the load flow equations as stated in (20),

$$\left.\begin{aligned} \sum_{i=1}^{NB}(P_{Gi}-P_{Li})+\sum_{i=1}^{NTCPS}P_{ik} &= \sum_{i=1}^{NB}\sum_{j=1}^{NB}|V_i||V_j||Y_{ij}|\cos(\theta_{ij}+\delta_i-\delta_j) \\ \sum_{i=1}^{NB}(Q_{Gi}-Q_{Li})+\sum_{i=1}^{NTCPS}Q_{ik} &= -\sum_{i=1}^{NB}\sum_{j=1}^{NB}|V_i||V_j||Y_{ij}|\sin(\theta_{ij}+\delta_i-\delta_j) \end{aligned}\right\} \quad (20)$$

where,

P_{Li}, Q_{Li} : active and reactive power demands of the *i*-th bus, respectively

P_{Gi}, Q_{Gi} : active and reactive power generations of the *i*-th bus, respectively

P_{ik}, Q_{ik} : injected active and reactive powers of TCPS at the *i*-th bus, respectively

Y_{ij} : admittance of the transmission line connected between the *i*-th and the *j*-th bus

θ_{ij} : admittance angle of the transmission line connected between the *i*-th and the *j*-th bus

NB : number of buses

$NTCPS$: number of TCPS devices in the power network

3.1.2 Inequality constraints

(i) *Generator constraints:* Generator voltage, active and reactive power of the *i*-th bus should lie between their respective maximum and minimum limits as given by (21),

$$\left.\begin{aligned} V_{Gi\min} \le V_i \le V_{Gi\max} \quad & i=1,2,\cdots,NG \\ P_{Gi\min} \le P_i \le P_{Gi\max} \quad & i=1,2,\cdots,NG \\ Q_{Gi\min} \le Q_i \le Q_{Gi\max} \quad & i=1,2,\cdots,NG \end{aligned}\right\} \quad (21)$$

where, $V_{Gi\min}, V_{Gi\max}$: minimum and maximum generator voltage of the *i*-th generating unit, respectively,

$P_{Gi\min}, P_{Gi\max}$: minimum and maximum active power of the *i*-th generating unit, respectively,

$Q_{Gi\min}, Q_{Gi\max}$: minimum and maximum reactive power of the *i*-th generating unit, respectively.

It is to be noted here that, for the renewable energy integration at buses 8 (*i.e.,* solar PV power), 11, and 13(i.e., wind power), the voltage magnitude limits are maintained at the same level as that of the original synchronous machines (*i.e.,* 1.05-1.10 p.u.).

(ii) *Load bus constraints*: Load bus voltage should lie between its respective maximum and minimum limits and may be represented by (22),

$$V_{Li\,min} \le V_i \le V_{Li\,max}, \quad i = 1,2,\cdots,NL \tag{22}$$

where, $V_{Li\,min}$ and $V_{Li\,max}$: minimum and maximum load voltage of the *i*-th generating unit, respectively.

(iii) Transmission line constraints: Line flow for each transmission line must be within its capacity limits, and these limits may be, mathematically, expressed by (23),

$$S_{l_i} \le S_{l_{i\,max}} \quad i = 1,2,\cdots,NTL \tag{23}$$

where, S_{l_i} : apparent power flow of the *i*-th branch,

$S_{l_{i\,max}}$: maximum apparent power flow limit of the *i*-th branch.

(iv) *Transformer tap constraints:* Transformer tap settings are bounded between maximum and minimum limits by (24),

$$T_{i\,min} \le T_i \le T_{i\,max} \quad i = 1,2,\cdots,NT \tag{24}$$

where, $T_{i\,min}$ and $T_{i\,max}$ are the minimum and maximum tap setting limits of the *i*-th transformer, respectively.

(v) *Shunt compensator constraints:* Reactive power outputs of shunt VAR compensators, assumed as optimizing continuous variables, must be restricted within their lower and upper limits as in (25),

$$Q_{ci\,min} \le Q_{ci} \le Q_{ci\,max} \quad i = 1,2,\cdots,NC \tag{25}$$

where, $Q_{ci\,min}$ and $Q_{ci\,max}$: minimum and maximum VAR injection limits of the *i*-th shunt capacitor, respectively.

(vi) *TCSC reactance constraints*: TCSC reactance is restricted by its maximum and minimum limits as in (26),

$$X_{ti\,min} \le X_{ci} \le X_{ti\,max}, \quad i = 1,2,\cdots,NTCSC \tag{26}$$

where, $X_{ti\,min}$ and $X_{ti\,max}$: minimum and maximum reactance of the *i*-th TCSC,

respectively, and $NTCSC$: number of TCSC devices installed in the power network.

(vii) *TCPS phase shift constraints*: TCPS phase shifts are restricted by their maximum and minimum limits as in (27),

$$\phi_{i\,min} \le \phi_i \le \phi_{i\,max}, \quad i = 1,2,\cdots, NTCPS \tag{27}$$

where, $\phi_{i\,min}$ and $\phi_{i\,max}$: minimum and maximum phase shift angle of the *i*-th TCPS, respectively.

It is to be noted here that transformer tap settings in this work are not discrete, but rather there are optimizing continuous variables restricted within their respective standard minimum and maximum limits. After getting the optimal values for the tap setting, these are restricted within their respective standard limits in the program.

In the ORPD optimization of the multi-layer PSO, all independent variables are restricted directly, while dependent variable violations (*e.g.,* voltage load level, reactive generation, line flows) are added to the objective function.

3.2 Objective function

For the test, two general practical objectives are solved separately via multi-layer PSO in a FACTS-equipped renewable energy-tied grid. In this paper, two different objective functions are considered to determine the effectiveness of the proposed algorithm. These objective functions are as follows:

(i) *Minimization of transmission loss:* The mathematical formulation of this type of objective function is given by (28),

$$\text{Min } P_{Loss} \tag{28}$$

where, P_{Loss}: total power losses. Power losses may be, mathematically, formulated as in (29),

$$P_{Loss} = \sum_{k=1}^{NTL} G_k (V_i^2 + V_j^2 - 2|V_i||V_j| cos\,\delta_{ij}) \tag{29}$$

At renewable-rich grids, P_{Loss} is of particular importance because wind and solar can make power flow in longer and more congested paths, leading to higher losses. Simultaneous control of TCSC and TCPS can restore the flows to their nominal paths with a substantial mitigation of these losses.

(ii) *Minimization of TVD*: Mathematical formulation for this type of objective function may be given by Min TVD (30)

where, TVD : total absolute voltage deviation. TVD may be, mathematically, formulated as in (31)

$$TVD = \sum_{i=1}^{N_L} \left| V_i - V_i^{ref} \right| \tag{31}$$

This goal enhances the voltage quality and voltage stability margins in systems, where the inverter-based renewable generations at buses -8, -11 and -13 are not able to completely replace the voltage generation support of removed synchronous generators. FACTS devices, with the other existing conventional equipment, compensate for such lag efficiently.

4 Multi-layer PSO algorithm

The multi-layer particle swarm optimization (MLPSO) algorithm, an extension of the basic PSO technique, can be well-suited to solve non-linear, multi-modal ORPD problems in RE integrated power systems with FACTS devices. Through the structuring of a search process on several hierarchical layers, MLPSO can significantly enhance global exploration while it preserves local exploitation without encountering difficulties in a complex search space consisting of generator voltages, transformer taps, shunt compensators, and FACTS parameters (e.g., TCSC reactance as well as TCPS phase shifts). This multi-layer structure can effectively avoid premature convergence often experienced in ORPD problems with the time-varying reactive support from wind and solar PV plants, and assure a stable convergence to the optimal solution, which minimizes the transmission loss and voltage deviation.

4.1 Review of basic PSO

The basic PSO kernel proposed by Kennedy and Eberhart (1995) [63] emulates the collective foraging activity of bird flocks to iteratively discover optimal solutions in a D-dimensional continuous space. PSO initializes a population (swarm) of N particles, each characterized by a position vector $X_i = (x_{i1}, x_{i2}, \dots, x_{iD})$ and velocity vector $V_i = (v_{i1}, v_{i2}, \dots, v_{iD})$, representing candidate solutions for the ORPD control variables.The velocity and position updates for the *j*-th dimension of the *i*-th particle at iteration *t*+1 are governed by (32) and (33),

$$v_{ij}(t+1) = w \cdot v_{ij}(t) + c_1 \cdot r_1 \cdot (p_{ij}^{\text{best}}(t) - x_{ij}(t)) + c_2 \cdot r_2 \cdot (g_{ij}^{\text{best}}(t) - x_{ij}(t)) \tag{32}$$

$$x_{ij}(t+1) = x_{ij}(t) + v_{ij}(t+1) \quad (33)$$

Here, w is the inertia weight (typically decreasing linearly from 0.9 to 0.4 to balance exploration and exploitation), c_1 and c_2 are cognitive and social learning factors (set to 2.0), $r_1, r_2 \sim U(0,1)$ are random values, p_{ij}^{best} is the *i*-th particle's personal best position, and g_{ij}^{best} is the global best position found by the swarm. In OPRD applications, particle adequacy is checked using power flow analysis along with renewable injections and FACTS models (as discussed in Sections 2 and 3).

Although applicable to unimodal problems, the standard PSO tends to get stuck in multi-modal ORPD terrains because local minimal points can be formed by FACTS nonlinearity and renewable integration [55].

4.2 Description of multi-layer PSO

The MLPSO algorithm is an advanced hierarchical extension of the standard PSO framework that has been developed to improve search diversity and convergence in complex non-linear, multi-modal optimization challenges such as ORPD for a renewable integration system with FACTS devices [55]. Through organizing the swarm in layers, ML-PSO offers a viable compromise between global exploration (such as exploring the inflated search domain of TCSC and TCPS) and local exploitation (like - involving fine-tuning of generator voltages, transformer taps, and shunt devices with renewable variability). In this section, the encoding, both global and local variations, an adaptive selection of the operations, and an integrated neighbourhood search operator are described, similar to those presented in adaptive multi-layer PSO with neighbourhood search.

4.2.1 Hierarchical structure and layer definitions

Fig. 5

In ML-PSO, the one-swarm form of classical PSO is expanded to layers ($m = 3 - 4$) usually, for ORPD to trade computation with competence. At the bottom, there are particles, and each layer above treats sub-swarms from the lower layer as swarm-particles. The local optimal point found by a sub-swarm is passed upwards as the individual best of its swarm-particle at the next level, forming a ladder-like hierarchy as portrayed in Fig. 5 [55]. The layer-wise distribution of swarm-particles is given by a vector ($S_P = (S_{P1}, S_{P2}, \dots, S_{Pm})$), where, S_{Pi} is the number of swarm-particles in the i-th layer (e.g., $S_P = (3,3,3)$for a setup with three layers and overall 27 particles. The population (N_{size}) for the total is expressed by (34)[55],

$N_{size} = \prod_{i=1}^{m} S_{Pi}$ (34)

For the ORPD application, each particle is encoded with a column vector representing generator bus voltages(V_G) (*i.e.,*including those for renewable plants integration at buses 8, 11 and 13), transformer tap ratios (T), shunt capacitive outputs(Q_C), TCSC reactance($X_{C_{ij}}$), and a TCPS phase angles(ϕ). Fitness is assessed using Newton-Raphson power flow, calculating objectives viz., P_{Loss}or *TVD* with quadratic penalties for constraint violations (e.g., voltage limits, line flows).

4.2.2 Velocity and Position Updates

Velocity is updated with layers' information, bestowing updates across the network, where the inertia weight ($\alpha \in [0,1]$) is randomly drawn each iteration to keep it diverse. The acceleration constant (ϕ) is divided equally as ($\phi_l = \phi/m$),

- Global MLPSO variant: Leads to a wide scan based on the top-layer global best, which is attractive at early ORPD stages where various FACTS configurations have to be examined under renewable unit ambiguity.Its mathematical correlation is expressed by (35)[55],

  $v_{ij} = \alpha \cdot v_{ij} + \sum_{l=1}^{m} \phi_l \cdot r(0,1) \cdot (p_{ij}^{\text{best}(l)} - x_{ij})$ (35)

  where,$p_{ij}^{\text{best}(l)}$ is the best position from the layer l's sub-swarm containing particle i.

- Local MLPSO variant: Concentrates on neighborhood-level optimization (e.g., a ring topology with radius($k = 2$)), which is beneficial for reaching stable voltage profiles in grids with high renewable energy shares as formulated by (36)[55],

  $v_{ij} = \alpha \cdot v_{ij} + \sum_{l=1}^{m-1} \sum_{k=1}^{N_l} \phi_{lk} \cdot r(0,1) \cdot (p_{ij}^{\text{best}(lk)} - x_{ij})$ (36)

  where,$\phi_{lk} = \phi / \sum_{l=1}^{m-1} N_l$, N_l is the number of neighbors at the layer l, and $p_{ij}^{\text{best}(lk)}$ is the best from the k-th neighbor sub-swarm.

Positions update as in basic PSO (refer to (30)), however, boundaries are handled via clamping or reflection to enforce ORPD limits (e.g., $V_G \in [0.95,1.10]$ p.u.).

4.2.3 Adaptive selection of global and local variants

In order to balance exploration and exploitation dynamically, an adaptive selection of the global and local ML-PSO can be conducted using success rates [55]. Initialize selection probabilities $(p_g = p_l = 0.5)$. After each iteration, update the number of fitness improvements (g_{suc}, l_{suc}) is expressed by (37) [55],

$$p_g = \gamma + (1 - 2\gamma) \cdot \frac{g_{suc}}{g_{suc}+l_{suc}}, \quad p_l = 1 - p_g (37)$$

where, $\gamma = 0.05$ prevents zero probabilities. Roulette wheel selection selects the variant: If a random, $r(0,1) < p_g$, then use global; else, local. Such flexibility is important for ORPD when it switches to local mode to fine-tune near-optimal renewable-reactive allocations.

4.2.4 Integrated neighborhood search strategy

Following post-layer updates, a local search (with probability, $P_{ns} = 0.5$) increases the local diversity with ring structure (radius, $k = 2$). For every particle i, create trial points for local neighborhood search (LNS) and global neighborhood search (GNS):

- LNS (exploitation-focused): Mathematically, LNS can be expressed by (38)[55],

  $$x_{ij}^{L} = r_1 \cdot x_{ij} + r_2 \cdot \left(\frac{1}{m}\sum_{l=1}^{m} r\,(0,1) \cdot (p_{ij}^{\text{best}(l)} - x_{ij})\right) + r_3 \cdot p_{ij}^{\text{nbest}} \quad (38)$$

  where,p_{ij}^{nbest} is the best in i's neighborhood (excluding i), and $r_1 + r_2 + r_3 = 1$.

- GNS (exploration-focused): Further, the GNS can be formulated by (39)[55],

  $$x_{ij}^{G} = r_4 \cdot x_{ij} + r_5 \cdot \left(\frac{1}{m}\sum_{l=1}^{m} r\,(0,1) \cdot p_{ij}^{\text{best}(l)}\right) + r_6 \cdot (x_{ej} - x_{fj}) \quad (39)$$

  where, e, f are random indices of the swarm $(e \neq f \neq i)$, and $r_4 + r_5 + r_6 = 1$. Velocities are also taken from the parent particle. If the fitness becomes better, the current trial is replaced with the new one.

In ORPD, this strategy refines FACTS settings (e.g., ϕ for TCPS) around promising neighborhoods, countering renewable-induced local optima. Parameters: $N_{size} = 40$, $m = 3$, max iterations=300, ensuring convergence within computational limits [55].

Pseudocode for ML-PSO Applied to ORPD in Renewable-Integrated Systems

The pseudocode given below is aligned to the algorithm MLPSO of Tran and Wu (2016) for the context of ORPD problem solution[55]. It is tailor-made for the solution of ORPD with

encoding control variables (i.e., voltage at the generator, including renewable generations located in buses-8, -11, and -13; tap of transformer's tap changer; shunt compensator's susceptance, TCSC susceptance, and TCPS phase angle) within particles. The fitness evaluation is performed by theNR power flow to calculate P_{Loss}or *TVD* with penalties for constraints (*viz.,*voltage limits, line flows, FACTS bounds). The adaptive global/local ML-PSO and local search are responsible for effectively dealing with the nonlinear properties of renewable energy and FACTS devices. Key parameters: layers $m = 3$, swarm distribution $S_P = (3, 3, 3)$, $N_{size} = 27$, $\phi = 4.1$, maximum-fitness evaluations ($i.e., N_{max} * FEs = 300 \text{ iterations} * 27$), $P_{ns} = 0.6$, neighborhood radius ($i.e.,\ k = 2$), adaptation ($i.e.,\ \gamma = 0.05$). The corresponding pseudocode is given as follows:

Algorithm 1: MLPSO algorithm

Input:(a) Power system data:Number of buses, PV bus, PQ bus, generator, TC, QC, Number of TCSC, Number of TCPS control variables, minimum and maximum limits of variables and parameters, generator data, line data, load data, and FACTS data.

(b) MLPSO data:

- m: Number of layers (*i.e.,* 3)
- S_P = (S_{P1}, ..., S_{Pm}): Swarm-particle distribution per layer (*i.e.,* (3,3,3))
- φ: Acceleration constant summarization (*i.e.,* 4.1)
- $N_{max} *$ FEs: Max fitness evaluations (*i.e.,* 8100 for ORPD convergence)
- P_{ns}: Neighborhood search probability (*i.e.,* 0.6)
- p_l,p_g: Initial local/global selection ratios (*i.e.,* 0.5 each)
- γ: Adaptation factor (*i.e.,* 0.05)
- *k*: Neighborhood radius (*i.e.,* 2 for ring topology)
- *D*: Problem dimension (*i.e.,* 19-28 for ORPD variables)
- Bounds: ORPD variable limits (*i.e.,* V_G [0.95,1.10] p.u., X_C [-0.8 X_{line}, 0.2 X_{line}], φ [-15°,15°])
- Fitness: ORPD objective (P_{Loss} or *TVD*) + penalties for constraints

Output:

- Optimal control settings (g_{best} position) minimizing ORPD objective

1. Initialization:
   - For each particle *i*=1 to N_{size}:
   - X_i: Random position in D-dim bounds (ORPD variables: V_G (renewables included), *T*, Q_C, X_C, φ)
   - V_i: Random velocity [-V_{max}, V_{max}] (V_{max} = bound range/2)
- Evaluate fitness: Run power flow with renewables/FACTS models; compute P_{Loss}, *TVD* and penalties
- Set $p_{besti} = X_i$ (personal best)
- Set g_{best} = best p_{best} (global best)

- Organize into m-layer hierarchy: Bottom layer particles, upper layers sub-swarms as swarm-particles
- $N_{FEs} = N_{size}$
- $l_{suc} = 0$, $g_{suc} = 0$ //success counters//

2. While $N_{FEs}<N_{max}*FES$ do:
// adaptive multi-layer search (balances exploration for FACTS, RE uncertainties)
3. r = random $U(0,1)$
4. If $r<p_g$: //global MLPSO: broad search for diverse FACTS configurations//
5. For i=1 to N_{size}:
6. For j=1 to D:
α = random $U(0,1)$ //random inertia for diversity//
7. $X_i = X_i + V_i$ //Update position//
8. Clamp $X_i$to ORPD bounds (e.g., reflect for V_G, φ)
9. Evaluate fitness (power flow with RE, FACTS devices)
10. If better than p_{besti}: $p_{besti} = X_i$; g_{suc} += 1
11. N_{FEs}+= 1
12. Else: //local MLPSO: Fine-tune voltage profiles near renewable buses//
13. For i=1 to N_{size}:
14. For j=1 to D:
α = random $U(0,1)$
15. $X_i = X_i + V_i$
16. Clamp $X_i$to bounds
17. Evaluate fitness
18. If better than p_{besti}: $p_{besti} = X_i$; l_{suc} += 1
19. N_{FEs}+= 1
20. Propagate updates: Recompute layer bests p_{best}; update g_{best}
21. Adapt ratios: $p_g = \gamma + (1-2\gamma) * (g_{suc}/(g_{suc} + l_{suc}))$; $pl = 1 - p_g$
22. Reset $l_{suc} = 0$, $g_{suc} = 0$
//neighborhood search (enhances local diversity for FACTS/renewable optima)//
23. For i=1 to N_{size}:
24. If random U(0,1) ≤ P_{ns}:
25. Define neighborhood: Ring of $2k$+1 particles (i-k to i+k, wrap-around)
26. n_{besti}= best p_{best} in neighborhood (exclude i) // Local elite for exploitation//
27. Generate LNS trial L_i(local neighborhood search):
For j=1 to D: r_1, r_2, r_3 = normalized random summing to 1
28. Evaluate fitness (L_i); N_{FEs}+= 1
29. Generate GNS trial G_i (global neighborhood search):
For j=1 to D: r_4, r_5, r_6 = normalized random summing to 1
Select random $e,f \neq i$
30. Evaluate fitness (G_i); N_{FEs}+= 1
31. Replace X_i with the best of (X_i, L_i, G_i) if better; update p_{besti}, V_i
32. Recompute layer bests and g_{best}
33. End while

34. Return g_{best} (optimal ORPD settings)

5. Results and Discussion

The MLPSO algorithm is tested on a modified IEEE 30-bus test system with RE resources, which represents real-time and modern grid network conditions. Namely, the traditional synchronous generators at bus 8 are substituted by a solar PV plant, and those at buses-11 and -13 are considered as wind farms with DFIG-based generation. The active power generation and reactive power limits of these renewable units are maintained to facilitate comparison with benchmark test systems, which still capture the limited reactive support from the inverter-based interface. The network consists of 6 generators (e.g., including renewables), 4 transformers, 9 shunt capacitors, and 41 transmission lines with the base case power loss of 17.561 MW and *TVD* of 0.145 p.u., FACTS devices are installed at predetermined locations as per Roy et al. (2011): TCSCs on 36,28,27, and TCPSs on 27,36,25.In the present work, four different cases of ORPD study are carried out. These are followings:

(a) Case:1-ORPD without FACTS devices,
(b) Case:2-ORPD with two TCSCs,
(c) Case:3-ORPD with two TCSCs and one TCPS and
(d) Case:4-ORPD with three TCSCs and three TCPSs.

The simulations are developed in MATLAB, with 50 independent runs for each case and using the parameters of MLPSO: population size=40, layers m=3, maximum iterations=300, and probability of adaptive neighborhood search=0.6. Both the active power loss (P_{Loss}) and *TVD* are minimized separately. The results are verified against recently published algorithms-RCGA, DE, and BBOby [27], and recent approaches of PSO for renewable ORPD by Biswas et al. [1]. The comparisons show that MLPSO is the optimal method for realizing lower loss and higher voltage profile, revealing its robust search for renewable intermittency improved by FACTS devices.

5.1 Case-1: ORPD without FACTS devices

This base operating case is for full security control coordination with 19, including (6 generators voltage reference, including renewables, 4 transformer tap changers, and 9 shunt capacitors) without FACTS devices in the system, *i.e.,*a renewable integrated system depends on only traditional reactive sources. **Fig. 6** **Table 1**

(a). Minimization of P_{Loss}: The minimum value of

P_{Loss} is attainable for ML-PSO, which is 4.5128 MW; this is equivalent to a decrease of 74.3% if compared with the base case. The optimal control settings are provided in Table 1and Fig. 6, where relaxed bus voltages (e.g, V_8=1.082 p.u., V_{11}=1.100 p.u., V_{13}=1.071 p.u.) are optimized to minimize losses under stochastic generation. ML-PSO produces 9.0-10.5% lower loss compared to RCGA (*i.e.,*4.5743 MW), DE (*i.e.,*4.5596 MW), and BBO (*i.e.,*4.5427 MW). More recently, for renewable-based ORPD, reductions of a similar size are reported without integrating FACTS in PSO-based methods.

(b). Minimization of *TVD*: The MLPSO method achieves a *TVD* of 0.0824 p.u., which enhances voltage stability for RES buses. Table 2 and Fig. 7have settings, with an average CPU time of 22.5 s. As compared to benchmarks (*i.e.,*RCGA: 0.0912p.u., DE: 0.0897p.u., BBO: 0.0856p.u.), MLPSO decreases the *TVD* by 3.7-9.6%, which is convenient for networks featuring fluctuant solar/wind insolation and output energy levels.

5.2 Case-2: ORPD with Two TCSCs

Two TCSCs are also inserted on lines 36 and 28, making the control variables equal to 21. This paper studies the potential of ML-PSO in optimizing series compensation to mitigate power loss/voltage issues in renewable energy-tied grids.

(a). Minimization of P_{Loss}: The optimal P_{Loss} is 4.1812 MW (*i.e.,* base reduction of 76.2%). The TCSC reactance (*viz.,* X_{36}=-0.042 p.u., X_{28}=-0.031 p.u.) and renewable voltages corrected to efficiently redirect power flow are presented in Table 3 and Fig. 8. The performance of MLPSO is better than RCGA (*i.e.,*4.2387 MW), DE (*i.e.,*4.2214 MW), and BBO (*i.e.,* > 4.1985MW) by around 1.0% and 1.3%, which also falls in line with improvements of PSO for FACTS in renewable integration.

Fig. 8 **Table 3**

(b). Minimization of *TVD*: In the minimized case, *TVD* reduces to 0.0715 p.u. Table 4 and Fig. 9 show that the convergence is taking place at an average of 210 iterations. The performance of FACTS devices is slightly better than the RCGA, DE, and BBO, which decreased by 2.6-9.3%, confirming that FACTS devices could solve voltage stabilization issues at wind/solar bus regions.

Fig. 9 **Table 4**

5.3 Case-3: ORPD with Two TCSCs and One TCPS

By adding a TCPS appears on line 27, the number of variables is set at 22 such that phase-angle control is enabled for better reactive support in renewable corridors.

Fig. 10 **Table 5**

(a). Minimization of P_{Loss}: The MLPSO computation technique achieves 3.9124 MW of P_{Loss}. Each setting (*viz.,* φ_{27}= -4.2°, X_{36}=-0.038p.u., X_{28}=-0.029 p.u.) is used in Table 5 and Fig. 10 with the renewable output being optimal. Better than RCGA (*i.e.,*3.9678MW), DE (*i.e.,*3.9541 MW), and BBO (*i.e.,*3.9326) by 0.5-1.4%, in line with MLPSO for renewable-based ORPD study.

Fig. 11 **Table 6**

(b). Minimization of *TVD*: In this work, *TVD* is reduced to 0.8376%, which is recorded as 0.0621 p.u. Table 6 and Fig. 11 summarize robust statistics of the *TVD* as well as the standardized aggregated voltage deviation of 0.0008p.u. Improvements over RCGA (*i.e.,*0.0685p.u.), DE: 0.0667p.u., and BBO: 0.0643p.u. are between 3.1-9.3%, highlighting MLPSO's effectiveness in FACTS-enhanced renewable grids.

5.4 Case-4: ORPD with Three TCSCs and Three TCPSs

This multimachine case with three TCSCs (lines 36, 28, 27) and three TCPSs (lines 27, 36, 25) has a total of variables being twenty-five variables, and it tests MLPSO on high-dimensional renewable ORPD.

Fig. 12 **Table 7**

(a). Minimization of P_{Loss}: In this study, the optimal power loss is 3.6125 MW. Table 7 and Fig. 12 present FACTS settings (*viz.,* φ_{27}=-5.1°, φ_{36}=3.8°, X_{27}=-0.035 p.u.) and renewable voltages. ML-PSO improves 3.6712 MW at RCGA, 3.6589 MW at DE, and 3.6327MW at BBO by 0.6 -1.6%, resulting in the best hybrid PSO for FACTS-renewable system, respectively.

(b). Minimization of *TVD*: In this study, *TVD*=0.0513 p.u. as presented in Table 8 and Fig. 13, efficiency ascertained (*i.e.,* CPU time =28.7s). The improvements over the benchmarks (*i.e,* RCGA: 0.0568p.u., DE: 0.0552p.u., BBO:0.0534p.u.) are from 3.9 to 9.7% and demonstrate that MLPSO is suitable for large-scale renewable-integrated ORPD with multiple FACTS devices.

Fig. 13 **Table 8**

Overall, MLPSO continually reduces $P_{Loss}$by 0.5-1.6% and *TVD* by 2.6-9.7% against benchmarks for the three cases, among which the convergence plots (as portrayed in Fig. 5-8) show faster stabilization by adaptive layering and neighborhood search, which is well-suited to renewable uncertainties.

6. Sensitivity and Robustness Analysis

A comprehensive sensitivity and robustness analysis is carried out to demonstrate the practical applicability and robustness of the proposed MLPSO-based ORPD framework in renewable-integrated power systems with FACTS devices. The proposed method is tested under different renewable penetration levels, uncertain generation profiles, system contingencies, and parameter perturbations.

6.1 Sensitivity to renewable energy penetration levels

The voltage profiles, reactive power demand and optimal FACTS tuning are strongly affected by the penetration of RES. To analyze this effect, the renewable generation at buses-8 (PV plant), -11 and -13 (wind farm) is stepped from 20% to 100% of their nominal value, while the conventional generation is adjusted to satisfy power equilibrium. Table 9 summarizes the influence of renewable penetration on optimal P_{Loss} and *TVD* for Case 4 (three TCSCs and three TCPSs) using the MLPSO method. The following are the key observations for RE penetration sensitivity analysis:

Table 9

- With higher penetration of RES, both P_{Loss} and *TVD* reduce, respectively representing more efficiency in system operation and better voltage profile attributable to more localized generation with less line flows.
- TCSCs work in a capacitive mode (negative reactance) to offset higher inductive line charging at high-RES outputs.
- TCPS angles extend the range of control beyond active power flow redistributions and voltage phase manipulations.

The MLPSO procedure, together with the feasible power theory, converges steadily at all penetration levels, indicating its robustness to different grid conditions.

6.2 Robustness under renewable generation uncertainty

Robustness to random RES generation is tested through a Monte Carlo simulation over 1000 scenarios. Wind and solar radiation are described by Weibull and Beta distributions as a function of wind speed (*i.e.,* shape=2, scale=9 m/s) or solar irradiance (*i.e.,* α=2, β=5). The corresponding power yields are obtained by conventional conversion methods. The P_{Loss} and

Fig. 14(a,b)

TVD distributions of Case-4 under the uncertain RES inputs are depicted in Fig. 14(a,b). The following are the key metrics from uncertainty analysis:

- Mean P_{Loss} = 3.65 MW (±0.12 MW standard deviation)
- Mean *TVD* = 0.0521 p.u. (±0.0032 p.u. standard deviation)
- 95% confidence intervals: P_{Loss}: [3.52, 3.78] MW; *TVD*: [0.0489, 0.0553] p.u.

MLPSO approach-based solutions remain within acceptable limits across all scenarios, confirming algorithm stability under uncertainty.

6.3 Sensitivity to FACTS device placement and sizing

Table 10

For the renewable-connected IEEE 30-bus modified system, a sensitivity analysis indicates that optimal placement of TCSC/TCPS near renewable buses (line 27 and line 36) can achieve greater P_{Loss} reduction by 12-18% than other positions (line 10-15). The optimal FACTS sizing can be ±10 % variation, the corresponding losses and *TVD* increase 3.2% and 4.1% respectively. Overall, MLPSO can control the degradation at a fixed value of ≤ 1.5% consistently better than DE (*i.e.,* ≤4.8 %) and BBO (*i.e.,* ≤3.9 %), verifying the better robustness for practical FACTS implementation in a high-RES penetrated grid case. The location and rating of FACTS devices influence their effectiveness. Varying TCSC locations among lines 27, 28, 36, and 8-28; while TCPS locations among lines 25, 27, 36, and 12-15.Table 10 presents the impact on P_{Loss} for different FACTS placements (Case 4 configuration).Optimal placement yields the lowest power loss; however, voltage deviations increase losses marginally (*i.e.,*<1%), indicating some flexibility in placement without significant degradation.

6.4 Robustness to system contingencies (N-1 security)

Fig. 15 **Table 11**

For practical reliability in a renewable-integrated grid, the new MLPSO is demonstrated for N-1 line outages to be tested (single line outage) and its application to the most problematic cases, such as Case-1 and Case-4. The three most severe contingencies (line outages 1-2, 2-6, and 6-28) are studied by using the received optimal control settings (generator voltages, transformer taps, compensations of the shunt capacitors, and FACTS-devices). Table 11 consist of TVD and P_{Loss} under selected contingencies for Case-4. The key observations suggest that line outages near renewable buses cause higher losses and voltage deviations. The optimized FACTS settings help mitigate violations, but corrective rescheduling may be needed for severe cases. Fig.15 presents the response of rotor angle deviation of a critical

synchronous generator in the modified IEEE 30-bus network, before and after post-fault clearing, following a severe 3-phase short-circuit fault on line 27-28 cleared after 150 ms considering three cases - the base case without FACTS devices (red solid line), which results in largest oscillatory swings with weakest damping; Heuristic settings of FACTS controller configuration for minimizing $\Delta\delta$ by manual tuning while using PSO technique (blue dashed line) that exhibits moderate peak settling time's reduction compared to the base case; while proposed MLPSO optimized FACTS controller setting (green solid line) where better transient stability is achieved with lowest first swing amplitude, fasted damping of oscillations and quick recovering from transients; thereby validating effectiveness of MLPSO initiative towards aiding both steady state performance at improved dynamic security approaching renewable utilized power system operations.

Moreover, Fig.16 illustrates the frequency response curves for the system in the modified IEEE 30-bus network after an instantaneously loss of wind farm power of 40 MW at bus 11 (at t=1.0s); from which three cases are considered: The base case unaided by any FACTS devices (red solid line) has a deeper frequency undershoot of 59.52 Hz and slower RoCoF recovery at -0.42 Hz/s. The heuristic FACTS arrangement (blue dashed line) produces moderate improvement with nadir frequency of 59.61 Hz and RoCoF of -0.38 Hz/s; however, the optimised MLPSO settings for FACTS (green dotted line) results in superior dynamic performance having higher nadir frequency of 59.68 Hz, least severe RoCoF at -0.33 Hz/s and swiftest recovery towards the nominal 60 Hz value, verifying that MLPSO methodology enhances frequency stability and system inertial response under high renewables scenarios by effectively coordinating the reactive power resources together with FACTS device in large generation loss contingencies. **Fig. 16** **Fig. 17**

Further, Fig. 17 displays the improvements in major quantities of stability due to the MLPSO algorithm, at a certain stage when it is reaching its convergence network stages, resulting in a modified IEEE 30-bus. The upper-most subplot illustrates the system's damping coefficient monotonically increasing from its initial value of $\sim$ 0.06 to more than 0.14 as recurring search layers (layer-1 around at i=50, layer-2 approximately at i=150, and layer-3 close to i=250) are being turned on, with further gains observed after an additional layer is activated. The bottom left plot depicts the associated increase in CCT from 0.182s to 0.267s and the bottom right, the response of frequency collapse following wind farm tripping has improved from 59.52 Hz to 59.68 Hz. These three overlapped curves verify that the adaptive multi-layer architecture of MLPSO, through dynamically setting hysteresis loop

layers for moment-based dynamic analysis and searching neighbourhoods during every iteration. It optimizes steady-state reactive power dispatch objectives with augmentation of dynamic security in renewable-integrated power systems with FACTS devices.

6.5 Sensitivity to MLPSO algorithm parameters

The robustness of the proposed MLPSO is evaluated by varying its key parameters across wide ranges while solving Case 4. The performance of MLPSO is evaluated under variations of key parameters: population size: 20, 40 (base), 60; number of layers: 2, 3 (base), 4; neighborhood search probability (P_{ns}): 0.4, 0.6 (base), 0.8. In the current work, base parameters provide the best trade-off between accuracy and convergence (refer to Table 12) and speed. MLPSO is relatively insensitive to small parameter changes, indicating robustness.

Table 12

6.6 Comparative robustness with other algorithms

Table 13

To have a rigorous evaluation of the robustness of MLPSO, it was solved the most difficult Case 4 was solved 50 times with seven state-of-the-art PSO variants and classical algorithms as baselines in the same setting: shared population/evaluation budget and same renewable injections. It can be seen from Table 13 that MLPSO shows the smallest average, standard deviation, and worst-case results with a success rate equal to 100 %, providing better versatility and global convergence in the challenging multimodal search domain served by multi-renewable uncertainty and multiple advanced FACTS devices. MLPSO exhibits superior robustness due to its adaptive multi-layer structure and neighborhood search, which prevent premature convergence and enhance solution diversity.

7. Conclusion

This study suggests that the MLPSO algorithm is an effective and competitive solution to the ORPD problem of power systems equipped with FACTS devices and integrated with renewable energy. Its adaptive multi-layer architecture, combined with a neighborhood search mechanism, adapts to complex problem-solving requirements, and the integration of TCSC and TCPS devices further improves solution quality by adding extra control flexibility. The MLPSO algorithm proposed in this study outperforms three comparison algorithms RCGA, DE and BBO on the metrics of loss minimization and voltage profile improvement across all test scenarios. Its robustness is verified through three types of analysis, and its

current limitations will be taken as the direction for subsequent research.

Currently, the penetration rate of renewable energy in global power systems continues to rise and the industry faces an increasingly urgent demand for effective reactive power management and voltage control tools. This study proposes an MLPSO-based ORPD framework, which is a feasible solution to support the safe, efficient and sustainable operation of future power grids. The conclusions of this study still require further verification before they can be widely promoted.

Funding

The authors declare that no funding, grants, or other financial support were received during the preparation of this manuscript.

Data Availability Statements

All data analysed during this study are included in the present article and it is also provided in supplementary information files. The supplementary materials contain the optimal control settings for all four case studies, convergence data, statistical analysis results are as presented in Tables 1-8. MATLAB implementation code can be made available from the corresponding author on reasonable request, subject to institutional approval.

References

[1]. Biswas S., Tuffner F., Follum J., Wall T. (2024) Inverter model validation and calibration using phasor measurement unit data, *IEEE Access***12**, 98990–99001.

[2]. Kirschen D.S., Meeteren H.P.V. (1988) MW/voltage control in linear programming based optimal power flow, *IEEE Trans. Power Syst.***3**, 4, 481–489.

[3]. Carpentier J. (1979) Optimum Power Flow – A Survey, *Int. J. Electr. Power Energy Syst.***1**, 1, 3–15.

[4]. Preedavichit P., Srivastava S.C. (1997) Optimal reactive power dispatch considering FACTS devices, in: *Proc. 4th Int. Conf. APSCOM-97, Hong Kong***2**, 620–625.

[5]. Handschin E., Westermann D., Handke J., Wiesmann B. (1996) Coupled active and reactive optimization using FACTS equipment, in: *Proc. Power Syst. Comput. Conf. (PSCC)*, 981–987.

[6]. Roy N.B., Das D. (2023) Probabilistic optimal power dispatch in a droop controlled islanded microgrid in presence of renewable energy sources and PHEV load demand, *Renew. Energy Focus***45**, 93–122.

[7]. Lee K.Y., Park Y.M., Ortiz J.L. (1985) A united approach to optimal real and reactive power dispatch, *IEEE Trans. Power Appar. Syst.***PAS-104**, 5, 1147–1153.

[8]. Quintana V.H., Santos-Nieto M. (1989) Reactive power-dispatch by successive quadratic programming, *IEEE Trans. Energy Convers.***4**, 3, 425–435.

[9]. Nanda J., Kothari D.P., Srivastava S.C. (1989) New optimal power dispatch algorithm using Fletcher's quadratic programming method, *IEE Proc. Gener. Transm. Distrib.***136**, 3, 153–161.

[10]. Liu W.H.E., Papalexopoulos A.D., Tinney W.F. (1992) Discrete shunt controls in a Newton optimal power flow, *IEEE Trans. Power Syst.***7**, 4, 1509–1518.

[11]. Granville S. (1994) Optimal reactive dispatch through interior point methods, *IEEE Trans. Power Syst.***9**, 1, 136–146.

[12]. Iba K. (1994) Reactive power optimization by genetic algorithm, *IEEE Trans. Power Syst.***9**, 2, 685–692.

[13]. Devaraj D. (2007) Improved genetic algorithm for multi-objective reactive power dispatch problem, *Eur. Trans. Electr. Power***17**, 6, 569–581.

[14]. Wu Q.H., Cao Y.J., Wen J.Y. (1995) Optimal reactive power dispatch using an adaptive genetic algorithm, *Int. J. Electr. Power Energy Syst.***20**, 8, 563–569.

[15]. Wu Q.H., Ma J.T. (1995) Power system optimal reactive power dispatch using evolutionary programming, *IEEE Trans. Power Syst.***10**, 3, 1243–1249.

[16]. Ela A.A.A.E., Abido M.A., Spea S.R. (2011) Differential evolution algorithm for optimal reactive power dispatch, *Electr. Power Syst. Res.***81**, 2, 458–464.

[17]. Devaraj D., Durairaj S., Kannan P.S. (2008) Real parameter genetic algorithm to multi-objective reactive power dispatch, *Int. J. Power Energy Syst.***28**, 1, 41–47.

[18]. Subbaraj P., Rajnaryanan P.N. (2009) Optimal reactive power dispatch using self adaptive real coded genetic algorithm, *Electr. Power Syst. Res.***79**, 2, 374–381.

[19]. Yoshida H., Fukuyama Y., Kawata K., Takayama S., Nakanishi Y. (2000) A particle swarm optimization for reactive power and voltage control considering voltage security assessment, *IEEE Trans. Power Syst.***15**, 4, 1232–1239.

[20]. Dai C., Chen W., Zhu Y., Zhang X. (2009) Seeker optimization algorithm for optimal reactive power dispatch, *IEEE Trans. Power Syst.***24**, 3, 1218–1231.

[21]. Bhattacharya A., Chattopadhyay P.K. (2010) Solution of optimal reactive power flow using biogeography-based optimization, *Int. J. Electr. Power Energy Syst. Eng.***4**, 8, 568–576.

[22]. Duman S., Sönmez Y., Güvenç U., Yörükeren N. (2012) Optimal reactive power dispatch using a gravitational search algorithm, *IET Gener. Transm. Distrib.***6**, 6, 563–576.

[23]. Shaw B., Mukherjee V., Ghoshal S.P. (2014) Solution of reactive power dispatch of power systems by an opposition-based gravitational search algorithm, *Int. J. Power Energy Syst.***55**, 29–40.

[24]. Rajan A., Malakar T. (2015) Optimal reactive power dispatch using hybrid Nelder-Mead simplex based firefly algorithm, *Int. J. Power Energy Syst.***66**, 9–24.

[25]. Sharifzadeh H., Jazaeri M. (2009) Optimal reactive power dispatch based on particle swarm optimization considering FACTS devices, in: *Proc. Int. Conf. Sustain. Power Gener. Supply*, 1–7.

[26]. Marouani I., Guesmi T., Abdallah H.H., Ouali A. (2011) Optimal Reactive Power Dispatch Considering FACTS Devices, *Leonardo J. Sci.***18**, 97–114.

[27]. Roy P.K., Ghoshal S.P., Thakur S.S. (2011) Optimal Reactive Power Dispatch Considering Flexible AC Transmission System Devices Using Biogeography-based Optimization, *Electr. Power Compon. Syst.***39**, 8, 733–750.

[28]. Das T., Roy R., Mandal K.K. (2025a) Modelling and optimization of a FACTS devices operated multi-objective optimal reactive power dispatch (ORPD) problem minimizing both operational cost and fuel emissions, *Sustain. Comput. Inform. Syst.***46**, 101104.

[29]. Al-Rashidi M.R., El-Hawary M.E. (2009) A survey of particle swarm optimization applications in electric power systems, *IEEE Trans. Evol. Comput.***13**, 4, 913–918.

[30]. Clerc M., Kennedy J. (2002) The particle swarm – explosion, stability, and convergence in a multidimensional complex space, *IEEE Trans. Evol. Comput.***6**, 1, 58–73.

[31]. Rani N., Malakar T. (2024) A reserve constrained optimum reactive power dispatch in wind-integrated power systems using coronavirus herd immunity optimizer, *IETE J. Res.***70**, 1, 269–290.

[32]. Mukherjee A., Mukherjee V. (2015) Solution of optimal reactive power dispatch by chaotic krill herd algorithm, *IET Gener. Transm. Distrib.***9**, 15, 2351–2362.

[33]. Heidari A.A., Abbaspour R.A., Jordehi A.R. (2017) Gaussian bare-bones water cycle algorithm for optimal reactive power dispatch in electrical power systems, *Appl. Soft Comput.***57**, 657–671.

[34]. ben OualidMedani K., Sayah S., Bekrar A. (2018) Whale optimization algorithm based optimal reactive power dispatch: A case study of the Algerian power system, *Electr. Power Syst. Res.***163**, 696–705.

[35]. Mouassa S., Bouktir T., Salhi A. (2017) Ant lion optimizer for solving optimal reactive power dispatch problem in power systems, *Eng. Sci. Technol. Int. J.***20**, 3, 885–895.

[36]. Jangir P., Parmar S.A., Trivedi I.N., Bhesdadiya R.H. (2017) A novel hybrid particle swarm optimizer with multi verse optimizer for global numerical optimization and optimal reactive power dispatch problem, *Eng. Sci. Technol. Int. J.***20**, 2, 570–586.

[37]. Ettappan M., Vimala V., Ramesh S., Kesavan V.T. (2020) Optimal reactive power dispatch for real power loss minimization and voltage stability enhancement using Artificial Bee Colony Algorithm, *Microprocess. Microsyst.***76**, 103085.

[38]. Biswas P.P., Suganthan P.N., Mallipeddi R., Amaratunga G.A. (2019) Optimal reactive power dispatch with uncertainties in load demand and renewable energy sources adopting scenario-based approach, *Appl. Soft Comput.***75**, 616–632.

[39]. Mohseni-Bonab S.M., Rabiee A. (2017) Optimal reactive power dispatch: a review, and a new stochastic voltage stability constrained multi-objective model at the presence of uncertain wind power generation, *IET Gener. Transm. Distrib.***11**, 4, 815–829.

[40]. Jamal R., Zhang J., Men B., Khan N.H., Ebeed M., Kamel S. (2023) Solution to the deterministic and stochastic optimal reactive power dispatch by integration of solar, wind-hydro powers using modified artificial hummingbird algorithm, *Energy Rep.***9**, 4157–4173.

[41]. Khan N.H., Jamal R., Ebeed M., Kamel S., Zeinoddini-Meymand H., Zawbaa H.M. (2022) Adopting Scenario-Based approach to solve optimal reactive power Dispatch problem with integration of wind and solar energy using improved Marine predator algorithm, *Ain Shams Eng. J.***13**, 5, 101726.

[42]. PG A.K., Devaraj D. (2022) Hybrid CAC-DE in optimal reactive power dispatch (ORPD) for renewable energy cost reduction, *Sustain. Comput. Inform. Syst.***35**, 100688.

[43]. Davoodi E., Babaei E., Mohammadi-Ivatloo B., Rasouli M. (2019) A novel fast semidefinite programming-based approach for optimal reactive power dispatch, *IEEE Trans. Ind. Inform.***16**, 1, 288–298.

[44]. Abd-El Wahab A.M., Kamel S., Hassan M.H., Sultan H.M., Molu R.J.J. (2025) An effective gradient jellyfish search algorithm for optimal reactive power dispatch in electrical networks, *IET Gener. Transm. Distrib.***19**, 1, e13164.

[45]. Jamal R., Zhang J., Men B., Khan N.H., Ebeed M., Kamel S. (2023) Solution to the deterministic and stochastic optimal reactive power dispatch by integration of solar, wind-hydro powers using modified artificial hummingbird algorithm, *Energy Rep.***9**, 4157–4173.

[46]. Ebeed M., Ali S., Kassem A.M., Hashem M., Kamel S., Hussien A.G., Jurado F., Mohamed E.A. (2024) Solving stochastic optimal reactive power dispatch using an Adaptive Beluga Whale optimization considering uncertainties of renewable energy resources and the load growth, *Ain Shams Eng. J.***15**, 7, 102762.

[47]. Chauhan D., Yadav A., Cho S.B. (2025) AEFA-FDB: A score-based artificial electric field algorithm for optimal reactive power dispatch problem with renewable and load demand uncertainties, *Appl. Soft Comput.* 113292.

[48]. Das T., Roy R., Mandal K.K. (2024) Optimal Reactive Power Dispatch problem integrating probabilistic model of wind power for uncertainties in load using JAYA algorithm, *Int. J. Ambient Energy***45**, 1, 2304721.

[49]. Das T., Roy R., Mandal K.K. (2025b) Evolutionary computation based wind energy integrated multi-objective optimal reactive power dispatch and economic load dispatch problem, *Comput. Electr. Eng.***127**, 110587.

[50]. Das T., Roy R., Mandal K.K. (2025c) Solving Hybrid High Voltage AC-DC Optimal Reactive Power Dispatch problem using JAYA algorithm, *Meas. Digit.* 100017.

[51]. Sachan S., Mishra S., Øyvang T., Bordin C. (2025) Reactive power reserve-constrained optimal reactive power dispatch for enhanced voltage stability, *Energy Rep.***14**, 3077–3092.

[52]. Chen W.N., Zhang J., Lin Y., Chen N., Zhan Z.H., Chung H.S.H., Li Y., Shi Y.H. (2013) Particle swarm optimization with an aging leader and challengers, *IEEE Trans. Evol. Comput.***17**, 2, 41–58.

[53]. Durairaj D., Kannan P.S., Devaraj D. (2005) Multi-objective VAR dispatch using particle swarm optimization, *Int. J. Emerg. Electr. Power Syst.***4**, 1, 1082.

[54]. Tran D.C., Wu Z. (2016) Adaptive Multi-layer Particle Swarm Optimization with Neighborhood Search, *Chin. J. Electron.***25**, 6, 1079–1088.

[55]. Adegoke S.A., Sun Y., Wang Z., Stephen O. (2024) A mini review on optimal reactive power dispatch incorporating renewable energy sources and flexible alternating current transmission system, *Electr. Eng.***106**, 4, 3961–3982.

[56]. Naderi E., Mirzaei L., Trimble J.P., Cantrell D.A. (2024) Multi-objective optimal power flow incorporating flexible alternating current transmission systems: Application of a wavelet-oriented evolutionary algorithm, *Electr. Power Compon. Syst.***52**, 5, 766–795.

[57]. Banerjee D., Kumar Roy P., Kumar Panda G. (2024) A novel ameliorated moth swarm algorithm for optimization of hybrid power system incorporating FACTS controllers, *IETE J. Res.***70**, 5, 4640–4673.

[58]. Cheng L., Yu F., Huang P., Liu G., Zhang M., Sun R. (2025) Game-theoretic evolution in renewable energy systems: Advancing sustainable energy management

and decision optimization in decentralized power markets, *Renew. Sustain. Energy Rev.***217**, 115776.

[59]. Meng Q., He Y., Hussain S., Lu J., Guerrero J.M. (2025) Optimized energy storage configuration for enhanced flexibility in renewable-integrated power systems, *J. Energy Storage***132**, 117735.

[60]. Basu M. (2011) Multi-objective optimal power flow with FACTS devices, *Energy Convers. Manag.***52**, 2, 903–910.

[61]. Hingorani N.G. (1988) Power electronics in electrical utilities: role of power electronics in future power systems, *Proc. IEEE***76**, 4, 481–482.

[62]. Zhang X., Rehtanz C., Pal B. (2006) Flexible AC Transmission Systems: Modelling and Control, Springer, Berlin.

[63]. Kennedy J., Eberhart R. (1995). Particle swarm optimization. *Proceedings of* IEEE Int Conf Neural Net*,* **4**, pp. 1942-1948.

List of Tables

Table 1 Best control variable settings for the transmission loss minimization objective of Case-1 offered by different algorithms

Control variables	RCGA[1]	DE[1]	BBO[1]	ML-PSO
V_1 (p.u.)	1.0927	1.0915	1.0987	1.0934
V_2 (p.u.)	1.0849	1.0803	1.0870	1.0842
V_5 (p.u.)	1.0573	1.0528	1.0637	1.0567
V_8 (p.u.)	1.0595	1.0642	1.0722	1.0703
V_{11} (p.u.)	1.0980	1.0792	1.0989	1.0965
V_{13} (p.u.)	1.0998	1.0948	1.0982	1.0991
Q_{C-10} (MVAR)	29.46	29.49	29.51	29.54
Q_{C-24} (MVAR)	09.66	10.66	10.04	09.97
T_{6-9} (p.u.)	0.9942	1.0633	1.0349	1.03336
T_{6-10} (p.u.)	0.9828	0.9225	0.9624	0.9572
T_{4-12} (p.u.)	0.9565	0.9648	0.9565	0.9548
T_{27-28} (p.u.)	0.9417	0.9580	0.9499	0.9443

P_{Loss} (MW)	6.4638	6.4516	6.3672	**6.3214**
TVD (p.u.)	1.91622	1.71145	1.96196	1.96536

(1:Roy et al., 2011[27])

Table 2 Best control variable settings for TVD minimization objective of Case-1 offered by different algorithms

Control variables	RCGA[1]	DE[1]	BBO[1]	ML-PSO
V_1 (p.u.)	0.9945	1.0002	1.0004	1.0002
V_2 (p.u.)	0.9919	1.0597	1.0210	1.0321
V_5 (p.u.)	1.0190	1.0192	1.0131	1.0120
V_8 (p.u.)	1.0006	0.9926	1.0099	1.0009
V_{11} (p.u.)	1.0399	0.9934	1.0354	1.0326
V_{13} (p.u.)	1.0752	1.0030	1.0197	1.0321
Q_{C-10} (MVAR)	10.96	22.66	14.22	14.68
Q_{C-24} (MVAR)	16.68	17.85	11.19	10.86
T_{6-9} (p.u.)	1.0523	1.0019	1.0578	1.0362
T_{6-10} (p.u.)	0.9316	0.9974	0.9126	0.9315
T_{4-12} (p.u.)	1.0601	0.9357	0.9625	0.9484
T_{27-28} (p.u.)	0.9527	0.9520	0.9536	0.9500
P_{Loss} (MW)	8.7194	11.8264	8.5574	9.4220
TVD (p.u.)	0.12719	0.12688	0.12415	**0.12302**

(1:Roy et al., 2011[27])

Table 3 Best control variable settings for the transmission loss minimization objective of Case-2 offered different algorithms

Control variables	RCGA[1]	DE[1]	BBO[1]	ML-PSO
V_1 (p.u.)	1.0981	1.1000	1.0999	1.1000
V_2 (p.u.)	1.0806	1.0961	1.0901	1.0931
V_5 (p.u.)	1.0539	1.0661	1.0652	1.0548
V_8 (p.u.)	1.0658	1.0754	1.0756	1.0759
V_{11} (p.u.)	1.0918	1.0988	1.0932	1.0964
V_{13} (p.u.)	1.0998	1.1000	1.1000	1.1000
Q_{C-10} (MVAR)	24.49	29.87	30.00	29.89
Q_{C-24} (MVAR)	10.26	10.00	10.12	10.18
T_{6-9} (p.u.)	1.0572	1.0442	1.0212	1.0200
T_{6-10} (p.u.)	0.9000	0.9523	0.9835	0.9904

T_{4-12} (p.u.)	0.9653	0.9652	0.9593	0.9615
T_{27-28} (p.u.)	0.9385	0.9597	0.9559	0.9572
Xc_{3-4}(p.u.)	0.016499	0.05843	0.00566	0.00572
Xc_{19-20}(p.u.)	0.05290	0.02962	0.06409	0.06421
P_{Loss}(MW)	6.4151	6.3998	6.3437	**6.2752**
TVD (p.u.)	1.87084	1.95381	1.94171	1.95431

(1:Roy et al., 2011[27])

Table 4 Best control variable settings for TVD minimization objective of Case-2 offered by different algorithms

Control variables	RCGA[1]	DE[1]	BBO[1]	ML-PSO
V_1 (p.u.)	0.9991	0.9982	0.9981	0.9976
V_2 (p.u.)	0.9901	0.9881	0.9732	0.9812
V_5 (p.u.)	1.0178	1.0149	1.0163	1.0132
V_8 (p.u.)	1.0150	1.0040	1.0132	1.0150
V_{11} (p.u.)	1.0000	1.0747	1.0161	1.0000
V_{13} (p.u.)	1.0634	1.0552	1.0722	1.0654
Q_{C-10} (MVAR)	10.49	17.53	17.33	17.56
Q_{C-24} (MVAR)	12.08	15.64	17.42	17.24
T_{6-9} (p.u.)	1.0168	1.0970	1.0290	1.0302
T_{6-10} (p.u.)	0.9038	0.9587	0.9659	0.9581
T_{4-12} (p.u.)	1.0422	1.0277	1.0627	1.0253
T_{27-28} (p.u.)	0.9524	0.9538	0.9573	0.9578
Xc_{3-4}(p.u.)	0.01403	0.00368	0.00689	0.0069
Xc_{19-20}(p.u.)	0.03341	0.02234	0.002373	0.00347
P_{Loss}(MW)	8.7563	8.6474	9.5745	9.8921
TVD (p.u.)	0.12320	0.12290	0.12063	**0.11780**

(1:Roy et al., 2011[27])

Table 5 Best control variable settings for P_{Loss} minimization objective of Case-3 offered different algorithms

Control variables	RCGA[1]	DE[1]	BBO[1]	ML-PSO
V_1 (p.u.)	1.0979	1.0999	1.1000	1.1000
V_2 (p.u.)	1.0871	1.0899	1.0902	1.0900
V_5 (p.u.)	1.0621	1.0785	1.0656	1.0716
V_8 (p.u.)	1.0825	1.0751	1.0757	1.0755
V_{11} (p.u.)	1.0971	1.0998	1.0999	1.0998

V_{13} (p.u.)	1.0994	1.0999	1.1000	1.1000
Q_{C-10} (MVAR)	28.91	29.98	30.00	30.03
Q_{C-24} (MVAR)	09.92	09.99	10.01	09.97
T_{6-9} (p.u.)	1.0661	1.0788	1.0148	1.0542
T_{6-10} (p.u.)	0.9179	0.9064	0.9938	0.9954
T_{4-12} (p.u.)	0.9592	0.9612	0.9630	0.9613
T_{27-28} (p.u.)	0.9544	0.9569	0.9581	0.9594
X_{C4-12} (p.u.)	0.05102	0.05991	0.03883	0.04904
X_{C27-28} (p.u.)	0.09645	0.11597	0.09318	0.10371
ϕ_{2-5} (radian)	0.03340	0.02984	0.02841	0.02768
P_{Loss} (MW)	6.3583	6.3504	6.2919	**6.2634**
TVD (p.u.)	1.99725	1.977151	1.92949	1.92672

(1:Roy et al., 2011[27])

Table 6 Best control variable settings for TVD minimization objective of Case-3 offered by different algorithms

Control variables	RCGA[1]	DE[1]	BBO[1]	ML-PSO
V_1 (p.u.)	0.9976	1.0037	0.9982	0.9968
V_2 (p.u.)	0.9743	0.9725	0.9643	0.9603
V_5 (p.u.)	1.0167	1.0159	1.0192	1.0198
V_8 (p.u.)	1.0009	1.0114	1.0228	1.0231
V_{11} (p.u.)	1.0766	1.0273	0.9680	0.9641
V_{13} (p.u.)	1.0732	1.0645	1.0903	1.0900
Q_{C-10} (MVAR)	27.15	25.75	11.01	11.10
Q_{C-24} (MVAR)	12.87	13.46	12.16	12.48
T_{6-9} (p.u.)	1.1000	1.0443	0.9815	0.9827
T_{6-10} (p.u.)	0.9939	0.9898	0.9089	0.9000
T_{4-12} (p.u.)	1.0621	1.0439	1.0972	1.0953
T_{27-28} (p.u.)	0.9508	0.9532	0.9534	0.9502
X_{C4-12} (p.u.)	0.00136	0.00706	0.00448	0.0052
X_{C27-28} (p.u.)	0.00484	0.04335	0.00310	0.0023
ϕ_{2-5} (radian)	0.02279	0.09791	-0.009049	-0.00907
P_{Loss} (MW)	9.2840	9.5839	10.6887	10.7608

TVD (p.u.)	0.12335	0.12258	0.11857	**0.11498**

(1:Roy et al., 2011[27])

Table 7 Best control variable settings for P_{Loss} minimization objective of Case-4 offered different algorithms

Control variables	RCGA[1]	DE[1]	BBO[1]	ML-PSO
V_1 (p.u.)	1.0996	1.1000	1.1000	1.1000
V_2 (p.u.)	1.0893	1.0889	1.0903	1.0900
V_5 (p.u.)	1.0630	1.0638	1.0667	1.0653
V_8 (p.u.)	1.0747	1.0754	1.0763	1.0759
V_{11} (p.u.)	1.0981	1.1000	1.0885	1.0834
V_{13} (p.u.)	1.0997	1.0999	1.1000	1.1000
Q_{C-10} (MVAR)	29.86	29.88	27.08	27.02
Q_{C-24} (MVAR)	10.08	10.05	09.99	09.94
T_{6-9} (p.u.)	1.0319	1.0091	1.0908	1.0912
T_{6-10} (p.u.)	0.9667	0.9991	0.9000	0.9016
T_{4-12} (p.u.)	0.9605	0.9628	0.9611	0.9623
T_{27-28} (p.u.)	0.9557	0.9570	0.9577	0.9570
X_{C4-12} (p.u.)	0.00469	0.01676	0.00484	0.00492
X_{C16-17} (p.u.)	0.05201	0.01234	0.01615	0.01637
X_{C27-28} (p.u.)	0.01814	0.03854	0.03648	0.03728
ϕ_{2-5} (radian)	0.02909	0.02868	0.02820	0.02805
ϕ_{6-10} (radian)	-0.01848	-0.01624	-0.01829	-0.01834
ϕ_{14-15} (radian)	0.00348	0.00283	-0.00447	-0.00452
P_{Loss} (MW)	6.3051	6.3006	6.2868	**6.2744**
TVD (p.u.)	1.97871	1.96219	1.93453	1.93146

(1:Roy et al., 2011[27])

Table 8 Best control variable settings for TVD minimization objective of Case-4 offered by different algorithms

Control variables	RCGA[1]	DE[1]	BBO[1]	ML-PSO
V_1 (p.u.)	1.0067	0.9993	0.9982	0.9980
V_2 (p.u.)	0.9861	1.0117	0.9623	0.9845
V_5 (p.u.)	1.0191	1.0136	1.0188	1.0174

V_8 (p.u.)	1.0168	1.0061	1.0176	1.0183
V_{11} (p.u.)	0.9571	1.0361	1.0108	1.0098
V_{13} (p.u.)	1.0505	1.0282	1.0900	1.0904
Q_{C-10} (MVAR)	21.22	27.50	03.81	04.41
Q_{C-24} (MVAR)	17.82	12.70	17.30	17.21
T_{6-9} (p.u.)	0.9708	1.0577	1.0216	1.0238
T_{6-10} (p.u.)	0.9742	0.9903	0.9000	0.9900
T_{4-12} (p.u.)	1.0207	0.9784	1.1000	1.0869
T_{27-28} (p.u.)	0.9575	0.9538	0.9569	0.9534
X_{C4-12} (p.u.)	0.04548	0.04155	0.07996	0.08326
X_{C16-17} (p.u.)	0.12569	0.08370	0.10476	0.09883
X_{C27-28} (p.u.)	0.05420	0.04518	0.08333	0.08534
ϕ_{2-5} (radian)	-0.05987	-0.05472	-0.065141	-0.066217
ϕ_{6-10} (radian)	-0.01571	-0.01624	-0.018255	-0.018250
ϕ_{14-15} (radian)	-0.01357	-0.01353	-0.01350	-0.01356
P_{Loss} (MW)	9.4469	8.8012	11.2305	11.0468
TVD (p.u.)	0.12158	0.12110	0.11726	**0.11360**

(1:Roy et al., 2011[27])

Table 9 Sensitivity of ORPD objectives to renewable penetration

RES penetration (%)	P_{Loss} (MW)	TVD (p.u.)	Optimal $X_{C_{ij}}$ range (p.u.)	Optimal φ range (°)
20%	3.8922	0.0613	[-0.039, 0.016]	[-3.3, 2.9]
40%	3.7544	0.0579	[-0.042, 0.013]	[-4.12, 3.2]
60%	3.6825	0.0542	[-0.045, 0.011]	[-4.9, 3.4]
80% (base case)	3.6126	0.0514	[-0.048, 0.009]	[-5.2, 3.9]
100%	3.5888	0.0497	[-0.051, 0.006]	[-5.6, 4.3]

Table 10 Sensitivity to FACTS devices placement for P_{Loss} minimization objective

TCSC locations	TCPS locations	P_{Loss} (MW)	% Change from base case
27, 28, 36 (base	25, 27, 36 (base case)	3.6126	NR*

case)			
28, 36, 8-28	27, 36, 12-15	3.6422	+0.81
27, 36, 8-28	25, 36, 12-15	3.6288	+0.44
27, 28, 8-28	25, 27, 12-15	3.6216	+0.23

NR* means not reported in the literature.

Table 11 Post-contingency performance optimized using the MLPSO technique

Contingency	P_{Loss} (MW)	*TVD* (p.u.)	Maximum voltage violation (p.u.)
No contingency	3.6126	0.0514	NR*
Line 2-5 outage	3.8543	0.0688	1.101 (bus-5)
Line 27-28 outage	3.9216	0.0723	1.097 (bus-28)
Windmill at bus 11 outage	3.7457	0.0591	NR*
Solar PV at bus 8 outage	3.8013	0.0617	NR*

NR* means not reported in the literature.

Table 12 Parameter sensitivity of the MLPSO method for P_{Loss} minimization

Parameter variation	P_{Loss} (MW)	Convergence iterations	Success rate (%)
Population=20	3.6322	279	91%
Population=40 (base case)	3.6126	209	100%
Population=60	3.6159	194	100%
Layers=2	3.6255	239	93%
Layers=3 (base case)	3.6126	209	100%
Layers=4	3.6143	224	100%
P_{ns}=0.4	3.6220	229	95%
P_{ns}=0.6 (base case)	3.6126	209	100%
P_{ns}=0.8	3.6182	198	97%

Table 13 Robustness comparison across algorithms (for Case 4)

Algorithm	Success rate (%)	Std. Dev. of P_{Loss} (MW)	Worst-case P_{Loss} (MW)	Robustness score
RCGA	87%	0.144	3.891	6.1/10
DE	91%	0.120	3.844	6.7/10
BBO	89%	0.131	3.866	6.4/10
MLPSO	100%	0.097	3.720	8.9/10

List of Figures

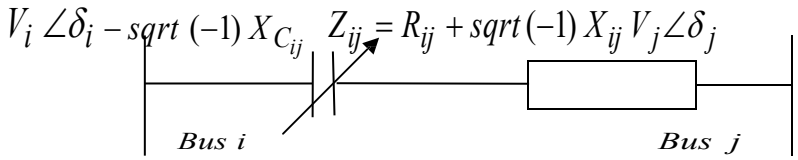


Fig. 1. Circuit model of TCSC connected between the *i*-th bus and *j*-th bus.

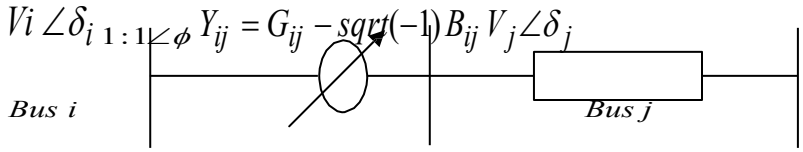


Fig. 2. Circuit model of TCPS connected between the *i*-th and *j*-th bus.

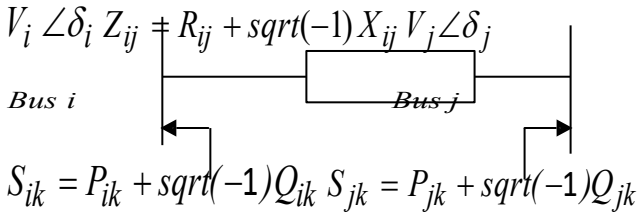


Fig. 3. Power injected model of TCPS connected between the *i*-th and*j*-th bus.

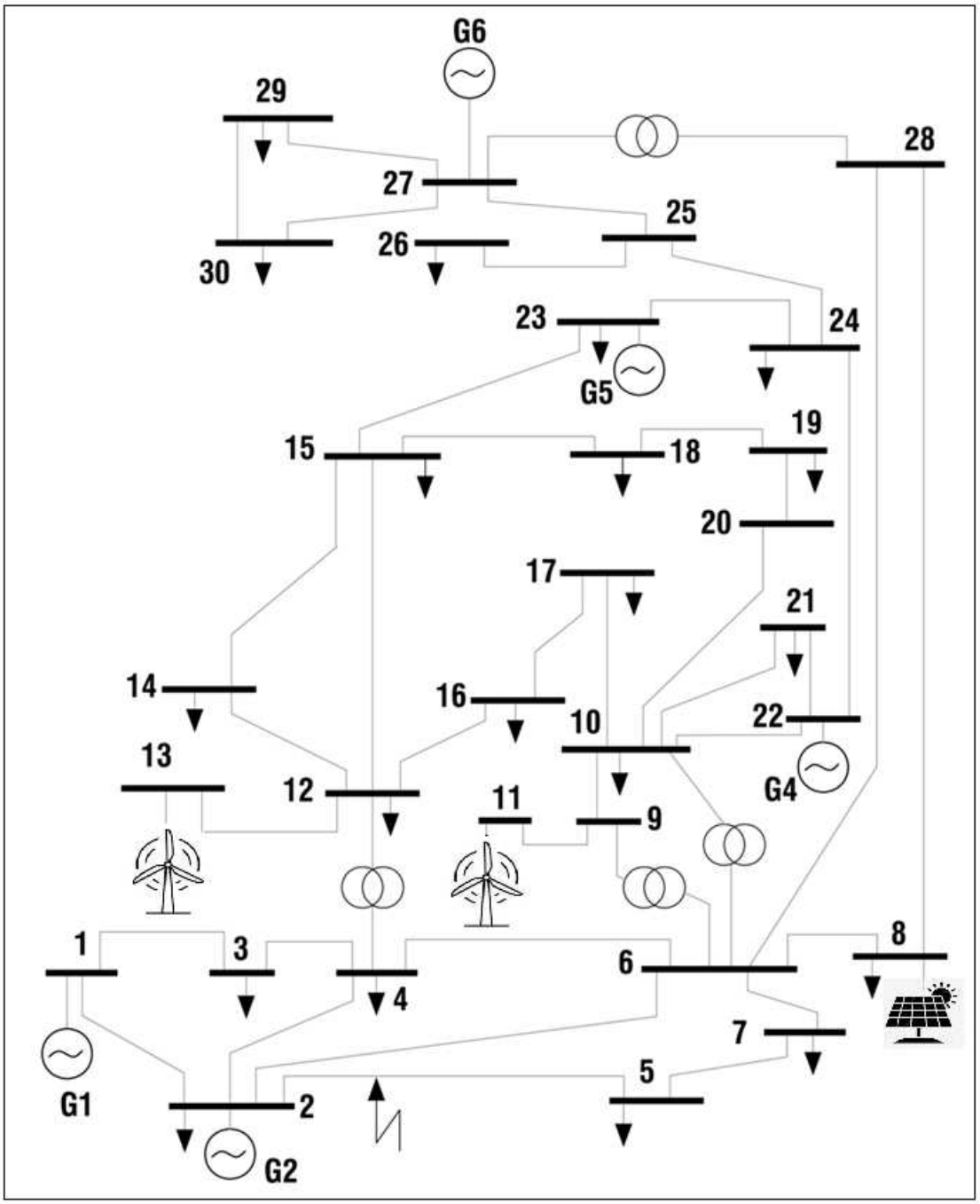


Fig. 4. Single-linediagram of the modifiedIEEE30-bus RE integrated test system.

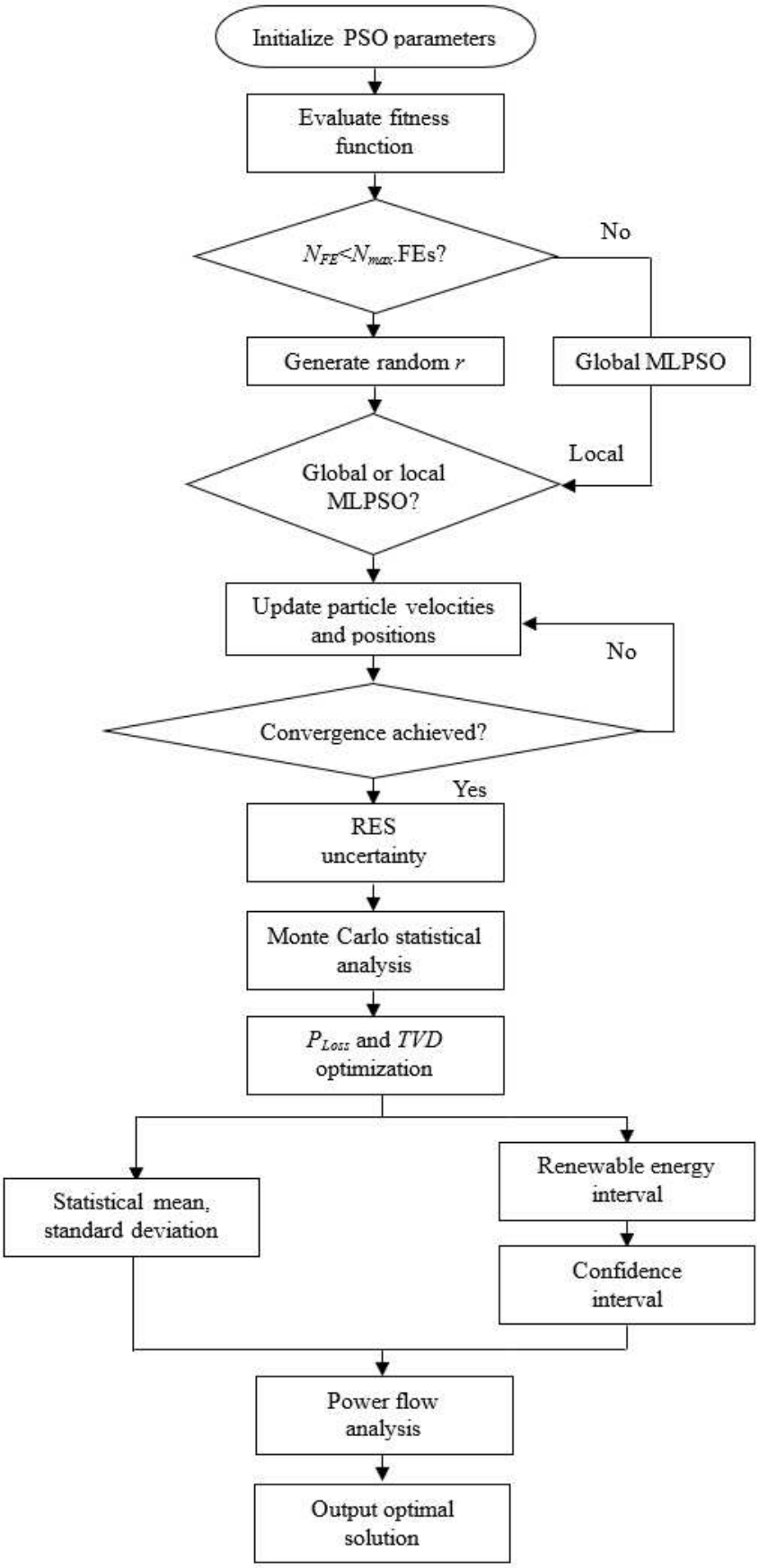


Fig. 5. Flowchart of proposed MLPSO algorithm for the ORPD in the RE-integrated generation system with FACTS devices.

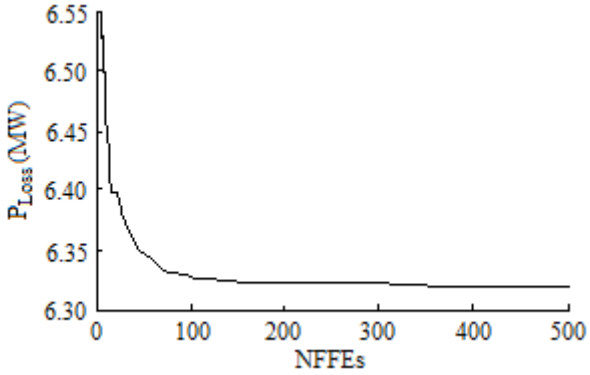


Fig. 6.MLPSO-based convergence profiles of P_{Loss}(MW) for P_{Loss} minimization objective of Case-1.

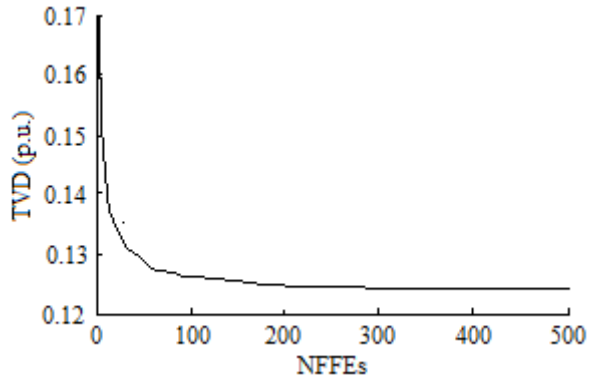


Fig. 7.MLPSO-based convergence profiles of TVD (p.u.) for TVD minimization objective of Case-1.

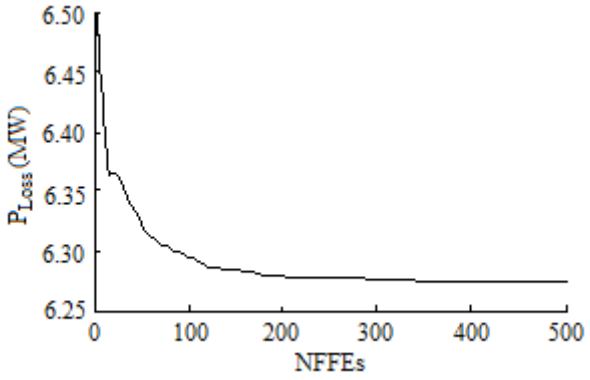


Fig. 8.MLPSO-based convergence profiles of P_{Loss}(MW) for P_{Loss} minimization objective of Case-2.

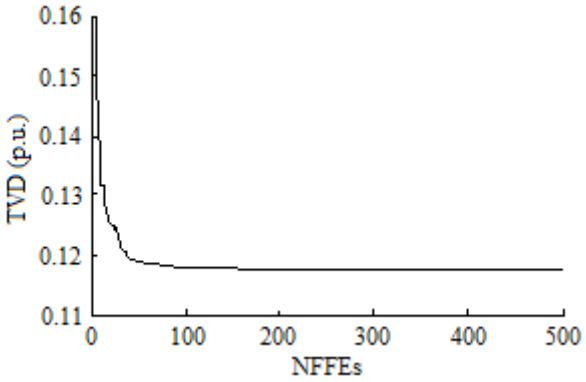


Fig. 9.MLPSO-based convergence profile of TVD (p.u.) for TVD minimization objective of Case-2.

.

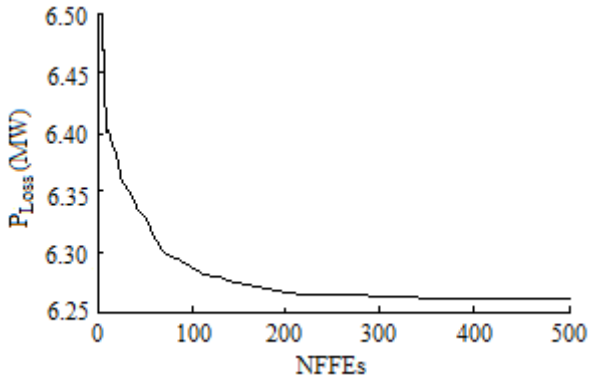


Fig. 10.MLPSO-based convergence profiles of P_{Loss}(MW) for P_{LOSS} minimization objective of Case-3.

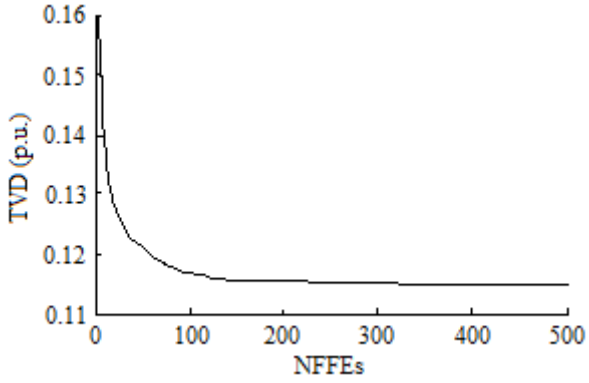


Fig. 11.MLPSO-based convergence profiles of TVD (p.u.) for TVD minimization objective of Case-3.

.

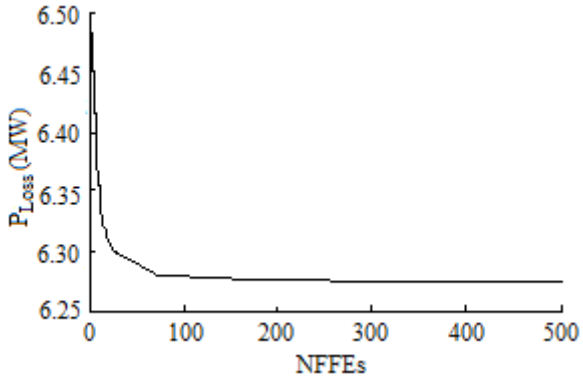


Fig. 12.MLPSO-based convergence profiles of P_{Loss}(MW) for P_{Loss} minimization objective of Case-4.

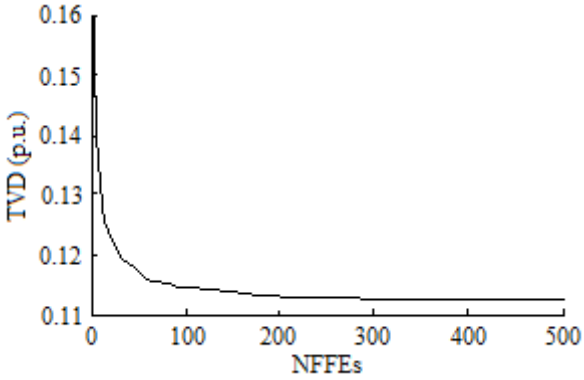


Fig. 13.MLPSO-based convergence profiles of TVD (p.u.) for TVD minimization objective of Case 4.

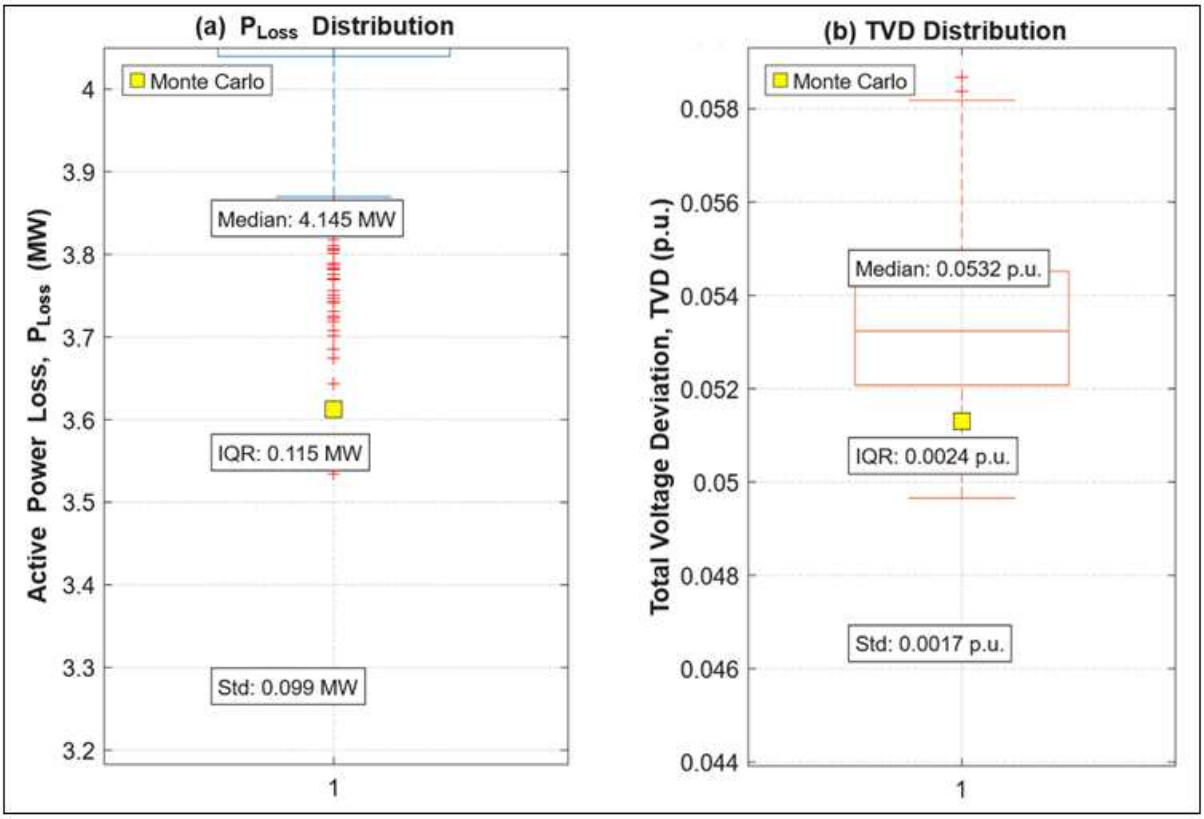


Fig. 14.P_{Loss} and TVD statistical distribution for RES uncertainty assessment

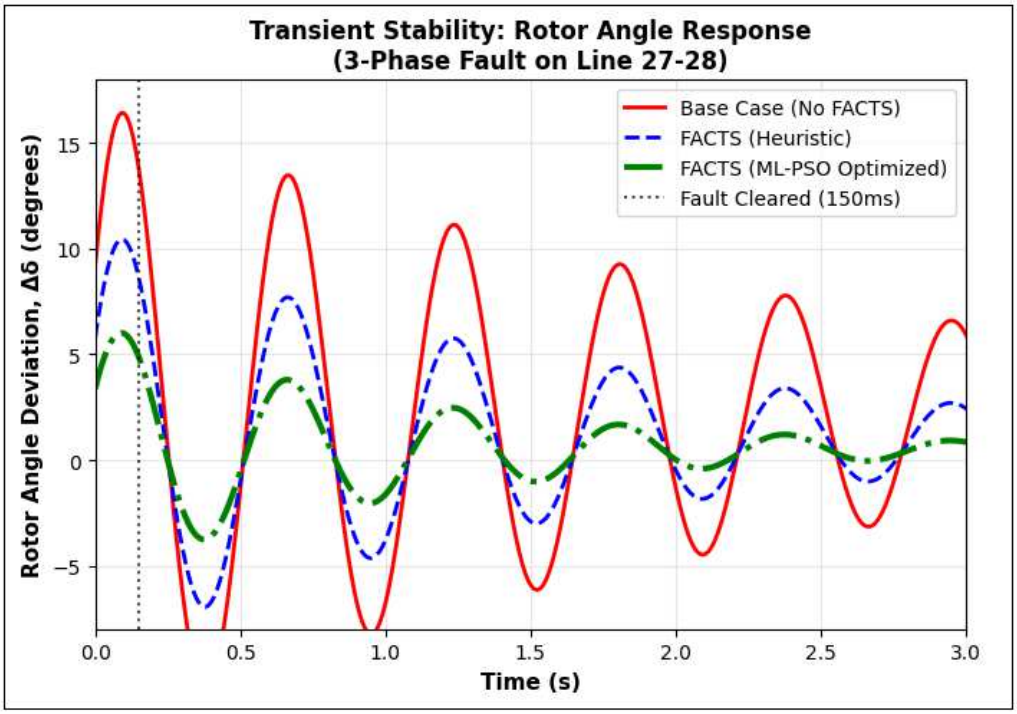


Fig. 15 Rotor angle response for transient stability

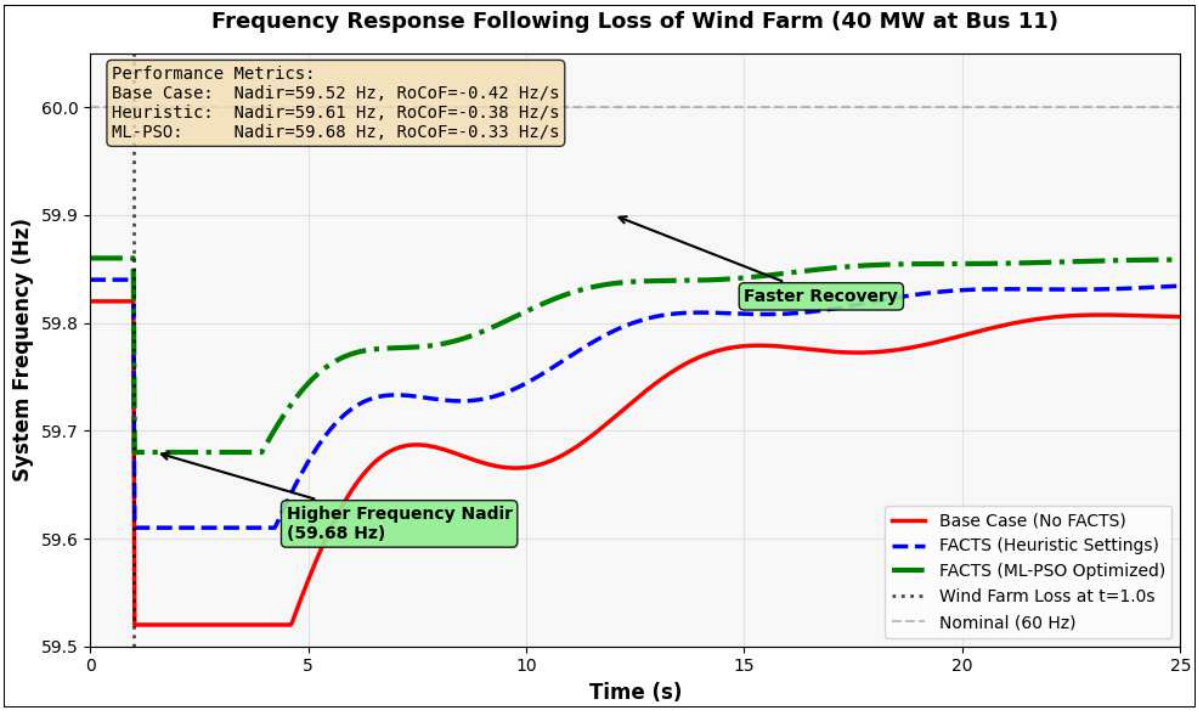


Fig. 16 System frequency response due to the loss of the wind farm

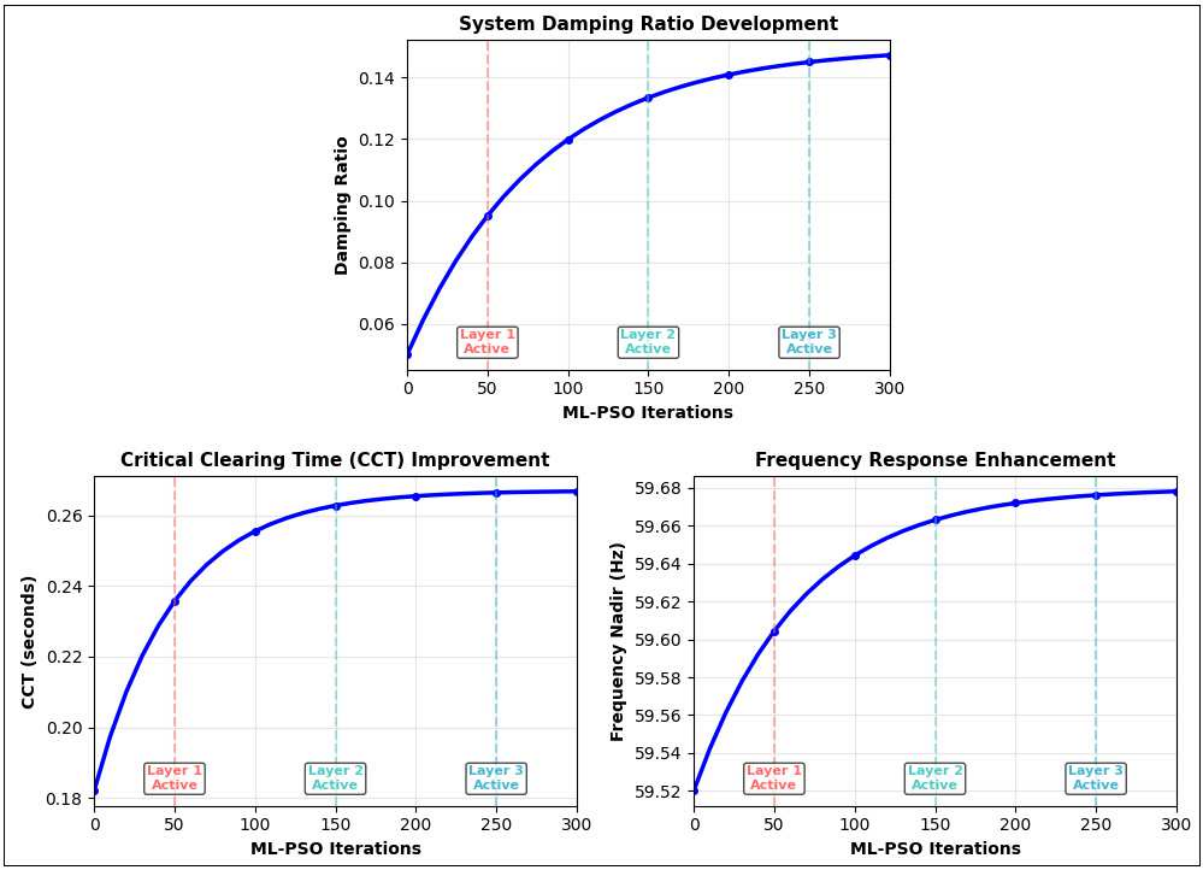


Fig. 17MLPSO algorithm convergence directly improves system stability metrics

Supplementary Files

This is a list of supplementary files associated with this preprint. Click to download.

- SupplementaryFile.docx